Published in "European Journal of Medicinal Chemistry 156 (): 760–773, 2018"
which should be cited to refer to this work.

Mononuclear silver(I) complexes with 1,7-phenanthroline as potent inhibitors of *Candida* growth

Nada D. Savić [a, 1], Sandra Vojnovic [b, 1], Biljana Đ. Glišić [a], Aurélien Crochet [c], Aleksandar Pavic [b], Goran V. Janjić [d], Marina Pekmezović [e], Igor M. Opsenica [f], Katharina M. Fromm [c, *], Jasmina Nikodinovic-Runic [b, **], Miloš I. Djuran [g, ***]

[a] *University of Kragujevac, Faculty of Science, Department of Chemistry, R. Domanovića 12, 34000 Kragujevac, Serbia*
[b] *Institute of Molecular Genetics and Genetic Engineering, University of Belgrade, Vojvode Stepe 444a, 11000 Belgrade, Serbia*
[c] *Department of Chemistry, University of Fribourg, Chemin du Musée 9, CH-1700 Fribourg, Switzerland*
[d] *Institute of Chemistry, Metallurgy and Technology, University of Belgrade, Njegoševa 12, 11000 Belgrade, Serbia*
[e] *Department of Microbial Pathogenicity Mechanisms, Hans Knöll Institute, Jena, Germany*
[f] *University of Belgrade-Faculty of Chemistry, Studentski trg 16, 11158 Belgrade, Serbia*
[g] *Serbian Academy of Sciences and Arts, Knez Mihailova 35, 11000 Belgrade, Serbia*

Mononuclear silver(I) complexes with 1,7-phenanthroline (1,7-phen), [Ag(NO_3-*O,O′*) (1,7-phen-*N7*)$_2$] (**1**) and [Ag(1,7-phen-*N7*)$_2$]X, X = ClO_4^- (**2**), $CF_3SO_3^-$ (**3**), BF_4^- (**4**) and SbF_6^- (**5**) were synthesized and structurally characterized by NMR (^{1}H and ^{13}C), IR and UV–Vis spectroscopy and ESI mass spectrometry. The crystal structures of **1, 3** and **4** were determined by single-crystal X-ray diffraction analysis. In all these complexes, 1,7-phen coordinates to the Ag(I) ion in a monodentate fashion *via* the less sterically hindered N7 nitrogen atom. The investigation of the solution stability of **1**–**5** in DMSO revealed that they are sufficiently stable in this solvent at room temperature. Complexes **1**–**5** showed selectivity towards *Candida* spp. in comparison to bacteria, effectively inhibiting the growth of four different *Candida* species with minimal inhibitory concentrations (MIC) between 1.2 and 11.3 μM. Based on the lowest MIC values and the lowest cytotoxicity against healthy human fibroblasts with selectivity index of more than 30, the antifungal potential was examined in detail for the complex **1**. It had the ability to attenuate *C. albicans* virulence and to reduce epithelial cell damage in the cell infection model. Induction of reactive oxygen species (ROS) response has been detected in *C. albicans*, with fungal DNA being one of the possible target biomolecules. The toxicity profile of **1** in the zebrafish model (*Danio rerio*) revealed improved safety and activity in comparison to that of clinically utilized silver(I) sulfadiazine.

1. Introduction

Candida albicans and emerging non-*albicans Candida* species, such as *C. parapsilosis*, *C. glabrata*, *C. tropicalis* and *C. krusei*, may cause infections ranging from superficial to life-threatening disseminated bloodstream and deep-tissue infections and account for ≥95% of all candidemia [1,2]. Existing therapies for the treatment of *Candida* infections rely on the use of several classes of compounds including polyenes, azoles, echinocandins, nucleoside analogs and allylamines with varying efficacy depending on the type and site of the infection, as well as susceptibility of the *Candida* species [3]. However, *Candida* species developed resistance to these conventionally used antifungal agents, leading to the treatment failures in patients and changes in the prevalence of species causing diseases [4]. The mechanisms of resistance to the antifungal drugs include an increased expression of drug efflux pumps which remove the drug from the cell before a toxic concentration can be reached, alteration of the structure or concentration of antifungal target proteins, and variation in the ergosterol biosynthetic pathways [5,6]. The problems associated with the developing resistance to the traditional therapy are a strong incentive for the search and

* Corresponding author.
** Corresponding author.
*** Corresponding author.
E-mail addresses: katharina.fromm@unifr.ch (K.M. Fromm), jasmina.nikodinovic@gmail.com (J. Nikodinovic-Runic), djuran@kg.ac.rs (M.I. Djuran).
[1] N.D.S. and S.V. contributed equally.

development of alternative antifungal agents.

Metal complexes might represent a novel class of antifungal agents due to their favorable features compared to the organic compounds, such as enhanced stereochemistry and reactivity, lipophilicity and redox potential [7] and possibly different modes of antifungal action. Among all metals of which complexes were found to be active against *Candida* species, silver has gained considerable attention due to its high toxicity to microorganisms and lower toxicity to mammalian cells [8]. The antimicrobial properties of silver(I) ions have been known from the ancient time and this metal ion represents an active agent in many healthcare products such as silver-coated catheters, wound dressings and burn-treatment creams [9–11]. An attractive class of ligands for the synthesis of silver(I) complexes as potential antifungal agents comprises aromatic nitrogen-containing heterocycles (*N*-heterocycles) [8,12–22]. For instance, 1,10-phenanthroline (1,10-phen) and its derivative, 1,10-phenanthroline-5,6-dione (1,10-phendio), and the respective silver(I) complexes of the general formula $[Ag(L)_2]ClO_4$ have been proven as very potent inhibitors of *C. albicans* growth [14–19]. The mode of their action has been examined and it was found that yeast cells after exposure to 1,10-phen and its silver(I) complex had a lower ability to reduce 2,3,5-triphenyltetrazolium chloride and, consequently, a reduced respiratory function [15,23]. Moreover, the $[Ag(1,10\text{-phen})_2]ClO_4$ reduced the levels of cytochromes aa_3, *b* and *c*, and led to a decrease in cellular ergosterol amount. As a consequence of all these processes, 1,10-phen and its silver(I) complex damaged mitochondrial function and uncoupled respiration [15]. The effect of these compounds on the structure of fungal and mammalian cell organelles has been also investigated and the obtained results showed that they were able to induce apoptosis in both types of cells [16]. On the other hand, 1,10-phendio and $[Ag(1,10\text{-phendio})_2]ClO_4$ caused extensive and non-specific DNA cleavage, gross distortions in fungal cell morphology and disruption of cell division [17,18].

The remarkable antifungal activity of silver(I) complexes with aromatic *N*-heterocycles, particularly with 1,10-phenanthroline, prompted us to synthesize and biologically evaluate silver(I) complexes with 1,7-phenanthroline (1,7-phen) (Scheme 1). In contrast to 1,10-phen, its structural isomer does not possess chelating properties; nevertheless 1,7-phen could behave as bridging ligand between two silver(I) ions by providing an acute 60° bridging angle [24]. However, due to the steric hindrance effect of the N1 nitrogen atom, 1,7-phen can also act as κ*N7* monodentate ligand exclusively [24,25]. A previous study related to the antifungal properties of 1,7-phen showed that, unlike 1,10-phen, this compound and their copper(II), manganese(II) and zinc(II) complexes displayed only marginal activity against *C. albicans* [14]. This was attributed to the fact that, although both 1,7- and 1,10-phen can coordinate to the metal center, only 1,10-phen was capable to chelate and form an extremely stable metal ion-phen moiety in solution [14]. Despite these findings and as a continuation of our efforts in the synthesis of biologically active silver(I) complexes with aromatic *N*-heterocycles [26–28], in the present study we have synthesized and structurally characterized five new silver(I) complexes with 1,7-phen, $[Ag(NO_3\text{-}O,O')(1,7\text{-phen-}N7)_2]$ (**1**) and $[Ag(1,7\text{-phen-}N7)_2]X$, $X = ClO_4^-$ (**2**), $CF_3SO_3^-$ (**3**), BF_4^- (**4**) and SbF_6^- (**5**) (Scheme 1). These complexes were assessed for *in vitro* antimicrobial and antiproliferative activities against the normal human lung fibroblast cell line (MRC5) to properly address their therapeutic potential. Considering the fact that complexes **1**–**5** have shown remarkable antifungal activity, the in depth antifungal potential, including the toxicity *in vivo* on zebrafish (*Danio rerio*) was also examined.

2. Results and discussion

2.1. Synthesis and structural characterization of the silver(I) complexes *1*–*5*

The silver(I) complexes with 1,7-phenanthroline, $[Ag(NO_3\text{-}O,O')(1,7\text{-phen-}N7)_2]$ (**1**) and $[Ag(1,7\text{-phen-}N7)_2]X$, $X = ClO_4^-$ (**2**), $CF_3SO_3^-$ (**3**), BF_4^- (**4**) and SbF_6^- (**5**), were synthesized according to the route presented in Scheme 1. The reaction of $AgNO_3$ with 1,7-phen in a 2: 1 mole ratio, respectively, in methanol/acetone (1: 1, v/v) at room temperature yielded mononuclear complex **1**. However, reactions of 1,7-phen with the other AgX salts ($X = ClO_4^-$, $CF_3SO_3^-$, BF_4^- and SbF_6^-), resulting in formation of the complexes **2**–**5**, were performed in ethanol by mixing an equimolar amount of the reactants. Despite the use of different silver(I) salts, 1,7-phen reacted with all to form similar mononuclear species, in which this *N*-heterocyclic ligand is monodentatedly coordinated to the Ag(I) ion through the less sterically hindered N7 nitrogen atom. The characterization of the complexes **1**–**5** was established on the basis of elemental analysis, NMR (^1H and ^{13}C), IR and UV–Vis spectroscopy and ESI mass spectrometry, while the crystal structures of **1**, **3** and **4** were determined by single-crystal X-ray diffraction analysis. Simultaneous attempts to crystallize complexes **2** and **5** from their amorphous powders using different solvents (water, methanol, acetone, chloroform, dimethylformamide) were unsuccessful.

2.1.1. Spectroscopic characterization

The NMR (^1H and ^{13}C), IR and UV–Vis spectroscopic data for the silver(I) complexes **1**–**5** are listed in the Experimental section (*vide infra*), alongside with the corresponding data for 1,7-phen. The proton NMR spectra for **1**–**5** measured in DMF-d_7 were noticeably different from that of the uncoordinated 1,7-phen. Monodentate coordination of 1,7-phen to Ag(I) ion changes its electronic properties, resulting in appearance of eight proton signals in the spectra of the complexes, instead of five in that of 1,7-phen. All proton signals of **1**–**5** are shifted downfield in respect to those of 1,7-phen. Which one of the two nitrogen atoms (N1 or N7) of 1,7-phen is coordinated to Ag(I) was deduced from the larger values of the observed chemical shifts (determined in respect to the free ligand) in the ^1H NMR spectra of the complexes. Thus, $\Delta(^1H)_{coord}$ values confirm that 1,7-phen coordinates to Ag(I) ion *via* the less sterically hindered nitrogen atom N7: $\Delta(^1H)_{coord}$ for H8 is larger than that for its counterpart, H2. However, one could observe only small shifts of the proton signals for complexes **1**–**5** with respect to those for 1,7-phen, what seems to be spectroscopic feature of silver(I) complexes in solution [29]. Although on the whole Ag(I) complexation of 1,7-phen produced an overall deshielding of ring carbons in **1**–**5**, the signals of several carbon atoms were shifted upfield. From the ^{13}C spectra of these complexes, one could also conclude that 1,7-phen is coordinated to Ag(I) through the N7 nitrogen, considering the largest shifts for the N7 adjacent carbons, C6 and C8, compared to the free ligand. On the other hand, the signals of the other carbon atoms are almost unaffected upon Ag(I) complexation.

The room temperature UV–Vis spectra of silver(I) complexes **1**–**5**, recorded in DMF/H_2O, resemble that of the 1,7-phen. In all complexes, the corresponding absorbance peak at ~269.0 nm, respectively, can be attributed to $\pi \rightarrow \pi^*$ transitions in phenanthroline [25,30] and they show slight red shift compared to that for the free ligand ($\lambda = 267.0$ nm).

The IR spectra of the complexes measured in the wavenumber range of 4000–450 cm^{-1} show the bands attributable to the vibration of the coordinated 1,7-phen, as well as those due to the corresponding counter-anion in the complexes **2**–**5** [31–36]. This is in accordance with the crystal structures of **3** and **4** determined by X-ray diffraction analysis (*vide infra*). Complex **2** exhibits a very

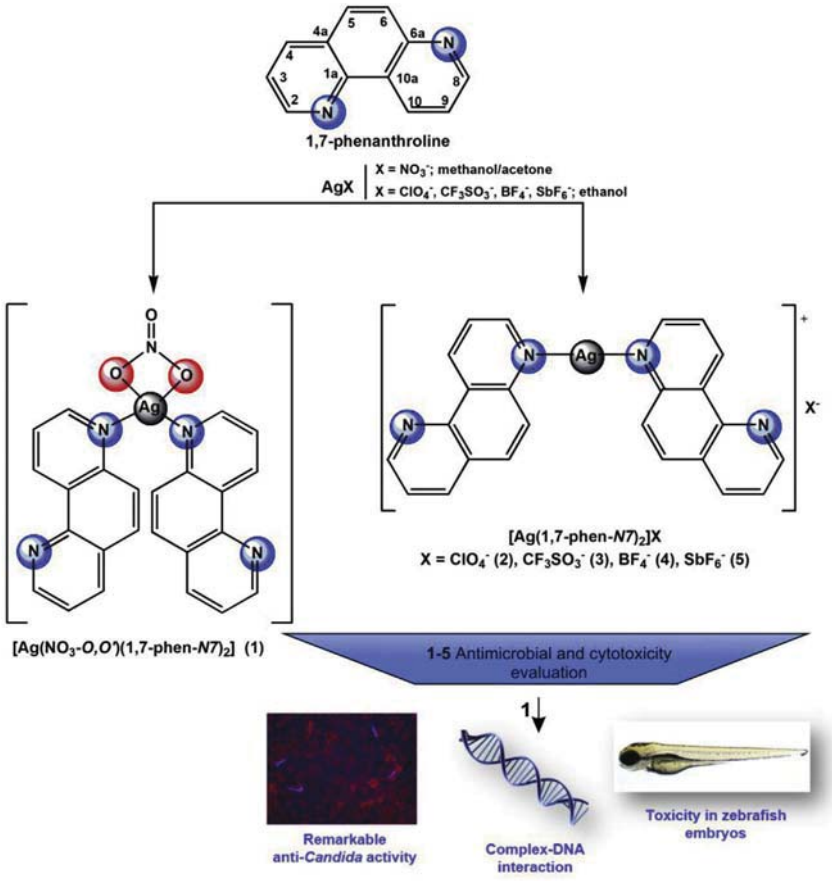

Scheme 1. Schematic presentation of the reactions for the synthesis of silver(I) complexes **1**–**5**. Numbering scheme of carbon atoms in 1,7-phen is in agreement with IUPAC recommendations for fused ring systems and does not match the one applied in the X-ray study of silver(I) complexes **1**, **3** and **4**. Considering the remarkable activity against all tested *Candida* species and lower cytotoxicity, complex **1** was selected for further activity analysis.

strong band with two sub-maxima at 1108 and 1064 cm^{-1} and a strong one at 622 cm^{-1} which can be attributed to the ν(ClO) and δ(OClO) modes, respectively, of the uncoordinated perchlorate [31]. The presence of the two bands attributed to the asymmetric stretching vibration of ClO_4^- ion can be the consequence of its participation in hydrogen bonding interactions, leading to its "pseudomonodentate" spectroscopic behavior [31,32]. As far as complex **5** is concerned, the presence of a strong band at 656 cm^{-1} in its IR spectra, indicates no coordination of SbF_6^- to the Ag(I) center [36]. On the other hand, a detailed analysis of the IR spectra of **1** [37,38], indicates that NO_3^- is bidentatedly coordinated to the Ag(I) ion in this complex.

ESI mass spectra. In the mass spectrometry of silver(I) complexes, the presence of two isotopes of nearly equal abundance, ^{107}Ag (51.84%) and ^{109}Ag (48.16%), is quite useful, because their mass spectra show doublet peaks with almost equal intensity for a mononuclear species or triplet peaks with approximately 1: 2: 1 intensity ratio, indicating the presence of dinuclear silver(I) species in solution [13,39]. The positive ion ESI mass spectra for **1**–**5** show two main doublet peaks centered at $m/z = 468.0$ and 361.0, consistent with theoretical m/z values calculated for $[Ag(1,7\text{-phen})_2]^+$ and [Ag(1,7-phen) (DMF)]$^+$ cations, respectively. This is in accordance with the presence of mononuclear silver(I) species also in solution.

2.1.2. Description of the single crystal structures

The molecular structures of the silver(I) complexes **1** and **4** with the anisotropic displacement ellipsoids and the atom numbering scheme are shown in Fig. 1, while their selected bond distances (Å) and valence angles (°) are listed in Table S1. This table also lists the corresponding structural parameters for complex **3**, which contains the same complex cation as **4**, but a different counter-anion (an ORTEP drawing of **3** is given in ESI, Fig. S1). As can be seen in Fig. 1, complex **1** is a mononuclear species comprising neutral [Ag(NO_3-*O,O'*) (1,7-phen-*N7*)$_2$] molecules. This complex has a strongly distorted tetrahedral geometry about the silver(I) ion, which is coordinated by two nitrogen atoms from two 1,7-phen ligands and by two oxygen atoms from the nitrate anion. The distortion can be revealed from the τ_4 parameter [40] of 0.67, $\tau_4 = [360^\circ - (\beta + \alpha)]/141^\circ$ where β and α are the largest angles around the metal ion (β = N1—Ag—N3 = 154.78(15)^o and α = N1—Ag—O2 = 110.83(15)^o). Perfectly square-planar and tetrahedral geometries result in τ_4 values of 0 and 1, respectively [40]. The two nitrogen atoms of the 1,7-phen ligands are at almost equidistance from the Ag(I) ion; the Ag—N1/N3 distances adopt values of 2.203(4) and 2.206(4) Å, respectively (Table S1) and compare well with those found in the other pseudo tetrahedral silver(I) complexes [27,41,42]. The Ag—O(nitrate) bond distances in **1** are in the range of 2.630(4) − 2.652(4) Å, being much longer than usual silver(I)-oxygen bonds of about 2.3 Å [43]. This indicates that the nitrate in **1** is only weakly bound to the silver(I) ion.

Similar to **1**, silver(I) complexes **3** and **4** contain two monodentatedly coordinated 1,7-phen ligands (Fig. 1 and Fig. S1). However, in contrast to **1**, the corresponding anions, *i.e.* triflate in **3** and tetrafluoroborate in **4**, are not coordinating to the metal center. Consequently, the Ag(I) ion adopts a slightly distorted linear geometry, with an N1—Ag1—N3 angle of 174.2(3) and 166.6(3)^o in **3**

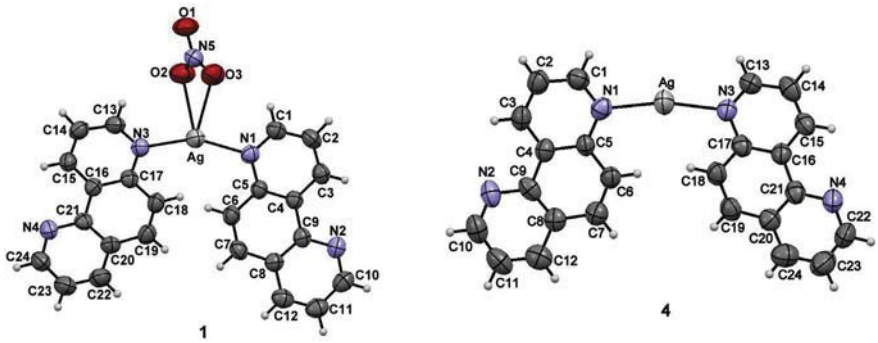

Fig. 1. Molecular structures of the silver(I) complexes **1** and **4**. Non-coordinating tetrafluoroborate anion in **4** is omitted for clarity. Displacement ellipsoids are drawn at 50% probability level and H atoms are represented by spheres of arbitrary size.

and **4**, respectively (Table S1). As in **1**, the nitrogen atoms of the two 1,7-phen ligands are at almost equidistance from the Ag(I) ion (Table S1) and are comparable with the other *N*-heterocycle-silver(I) complexes [26,27,41,42].

2.2. Stability of complexes

The solution behavior of silver(I) complexes **1**–**5** was analyzed by ^{1}H NMR spectroscopy. For this purpose, these complexes were dissolved in DMSO-d_6, and their ^{1}H NMR spectra were recorded directly after dissolution and after 48 h standing in the dark at room temperature. For all complexes, ^{1}H NMR spectra remained unmodified over 48 h, implying their substantial stability in solution during that time. More specifically, no decomposition of the complexes to the free 1,7-phen and no coordination of DMSO to the Ag(I) ion were observed. As an illustration, the NMR spectra of **3** are presented in Fig. S2 as a function of time.

In order to investigate the air/light stability of the silver(I) complexes which might be of importance for their use as antimicrobial agents in the form of ointments, gels and coating materials of dressings [29], sterile cellulose discs impregnated with these complexes (5 μL of 50 mg/mL DMSO stock solution) were exposed to air and light for 48 h (Fig. S3). As can be seen from Fig. S3, all investigated silver(I) complexes started to be a little beige in color after 24 h, and after 48 h all were darker, indicating that slow light decomposition processes occurred during this time.

2.3. Biological activity of the silver(I) complexes

2.3.1. Antimicrobial activity

Silver(I) complexes **1**–**5** and the corresponding 1,7-phen ligand were evaluated for their activity against five bacterial strains, including Gram-negative *Escherichia coli*, *Pseudomonas aeruginosa*, *Klebsiella pneumoniae*, and Gram-positive *Staphylococcus aureus* and *Enterococcus faecalis* as well as four *Candida* spp. (*C. albicans*, *C. parapsilosis*, *C. glabrata* and *C. krusei*). Their antibacterial activity was compared with the antibacterial properties of silver(I) sulfadiazine (AgSD), a topical antibiotic used in partial thickness and full thickness burns to prevent infection for more than 40 years [44,45]. MIC values against bacterial strains for silver(I) complexes **1**–**5** were between 25 and 125 μM (Table 1). The investigated silver(I) complexes showed considerably higher antibacterial potency compared to the starting 1,7-phen ligand, however, their MIC values in comparison to that of AgSD were either comparable or higher, indicating moderate antibacterial activity (Table 1). These MIC values are comparable with that of silver(I) complexes of 2,2′-bipyridine and 1,10-phenanthroline [22]. On the other side, **1**–**5** showed considerable antifungal activity against all tested *Candida* strains, with *C. krusei* and *C. albicans* being the most sensitive. Antifungal activity was comparable or better to that of AgSD, with MIC concentrations between 1.2 and 11.3 μM (Table 1). Especially, in the case of complex **1** that showed 5-fold lower MIC value against *C. albicans* and 4-fold lower cytotoxicity, in comparison to AgSD (Table 1). Generally, **1**–**5** were moderately cytotoxic against healthy human fibroblasts, with selectivity index in respect to anti-*Candida* activity for **1** being ≥30 in the case of *C. parapsilosis* (Table 1). Such remarkable anti-*Candida* activity has been observed for $[Ag_2(1,10\text{-phen})_3(mal)]\cdot 2H_2O$, $[Ag(1,10\text{-phen})_2]ClO_4$ and $[Ag(1,10\text{-phendio})_2]ClO_4$ complexes, whereby starting 1,10-phenanthroline and 1,10-phenanthroline-5,6-dione ligands also exerted strong antifungal activity [14–19]. On the contrary, 1,7-phen had only marginal antifungal effect (Table 1). Moreover, the most anti-*Candida* active $[Ag(1,10\text{-phendio})_2]ClO_4$ complex was toxic to the non-neoplastic cell lines, suggesting its inability to selectively kill fungal cells, while leaving the normal cells viable [19].

Table 1
Antimicrobial activity of silver(I) complexes **1**–**5**, 1,7-phen and silver(I) sulfadiazine (AgSD), in comparison to their antiproliferative effect on healthy human fibroblast MRC5 cell line.

Minimal inhibitory concentrations (MICs, μM)							
Test organism	**1**	**2**	**3**	**4**	**5**	1,7-phen	AgSD
E. coli	75[a]	80	80	100	70	500	50
P. aeruginosa	50	25	80	25	40	500	25
K. pneumoniae	100	88	80	100	80	500	75
S. aureus	125	100	80	90	125	500	75
E. faecalis	80	44	42	45	40	500	100
C. albicans	1.8	5.5	10.1	5.6	4.4	500	10
C. parapsilosis	1.2	11.0	10.1	11.3	8.9	500	2.5
C. glabrata	10	11	10.1	11.3	8.9	600	5.1
C. krusei	2.5	5.5	5.1	5.6	8.5	500	2.5
MRC5 cells	40[b]	15	25	12.5	20	135	10

[a]Results are given as mean of three independent measurements with standard error being between 1 and 3%.
[b]Calculated IC_{50} values correspond to concentrations required to inhibit 50% of cell growth.

In contrast to the complexes **1**–**5**, the previously synthesized silver(I) complexes with aromatic *N*-heterocycles having two nitrogens within one ring, such as diazines (pyridazine, pyrimidine, pyrazine), benzodiazines (phthalazine, quinazoline, quinoxaline) and tricyclic phenazine, showed considerable antibacterial activity, while their efficacy in inhibiting *C. albicans* growth was moderate [26–28]. These complexes were particularly efficient against pathogenic *P. aeruginosa*, and had a marked ability to disrupt clinically relevant biofilms of strains with high inherent resistance to antibiotics [27,28]. However, they were more cytotoxic against healthy human fibroblasts than most of the presently reported

complexes [26–28].

Considering the improved therapeutic window and the remarkable activity against all tested *Candida* species coupled with the fact that structural differences to other complexes were in the different counter ion, **1** was selected for further activity analysis.

2.3.2. Anti-Candida activity of **1**

2.3.2.1. Effect on C. albicans SC5314 virulence in epithelial infection model. *In vitro* epithelial cell models are well established to study different stages of infection, from adhesion to the host cells, *via* hyphal formation finally damage of the hosts cells by contact-sensing, directed hyphal extension, active penetration and secretion of the newly discovered toxin candidalysin [46,47]. For **1** and silver(I) sulfadiazine (AgSD), MIC ± one dilution was tested in oral epithelial cell model with human TR-146 cells where invasion (hyphal length) and the damage of the host cells were assessed (LDH release; LDH is lactate dehydrogenase) (Fig. 2). So far, copper(II) and zinc(II) complexes with 2,2′-bipyridine were reported to interact and inhibit LDH protein [48].

The presence of the MIC concentrations of **1** and AgSD reduced the hyphal length similarly by 10–15% in comparison to untreated control (Fig. 2A and B). At the concentrations one dilution higher than MIC, both complexes had similar efficiency in reducing the damage (24–30% reduction, Fig. 2C). However, in MIC and sub-MIC concentrations, the presence of **1** leads to the higher reduction of epithelial damage comparing to AgSD (Fig. 2C). A relatively moderate reduction of damage, in general, could be explained by the fact that the epithelial damage is measured 24 h post-infection and it could be that *C. albicans* develops certain adaptations and initiates other pathogenicity mechanisms which still leads to the damage despite the presence of the compounds.

2.3.2.2. Reactive oxygen species (ROS) generation in C. albicans. The fungicidal activity of antifungal compounds is often attributed to the ROS production [49]. Generation of ROS in *C. albicans* treated with 2-fold MIC concentrations of silver(I) complex **1**, 1,7-phen, AgSD and amphotericin B (AmB) was quantified using 2′,7′-dichlorofluorescin diacetate (DCFH-DA) staining and indicated by 2′,7′-dichlorofluorescein (DCF) fluorescence due to DCFH-DA probe oxidation (Fig. 3). Quantification of cellular ROS generation by flow cytometry revealed more pronounced increase in DCF fluorescence after 1.5 h of incubation with silver(I) complex **1** compared to AmB, clinically used antifungal, known for its ability to induce apoptosis and hence ROS production in *C. albicans* [49] (Fig. 3). Generation of ROS in *C. albicans* treated with 1,7-phen was almost the same as the control sample, cells treated with DMSO. Notably, the effect of AgSD on the ROS generation in *C. albicans* was 30-fold higher in comparison to both **1** and AmB. This may not be surprising, as AgSD has been connected with numerous side effects and toxicity [50]. Taken together, these results suggest that eradication of *Candida* induced by silver(I) complex **1** could be due to ROS production upon prolonged exposure, being in accordance with the previously published findings for the mechanism of action of silver(I)-containing species [51].

2.3.3. In vitro DNA binding and molecular docking

We have examined the possibility that ROS generation observed in *C. albicans* treated with **1** (Fig. 3) may be due to the initial interaction with fungal DNA. The prediction of drug binding to DNA at molecular level, provided by molecular docking, is the basis of

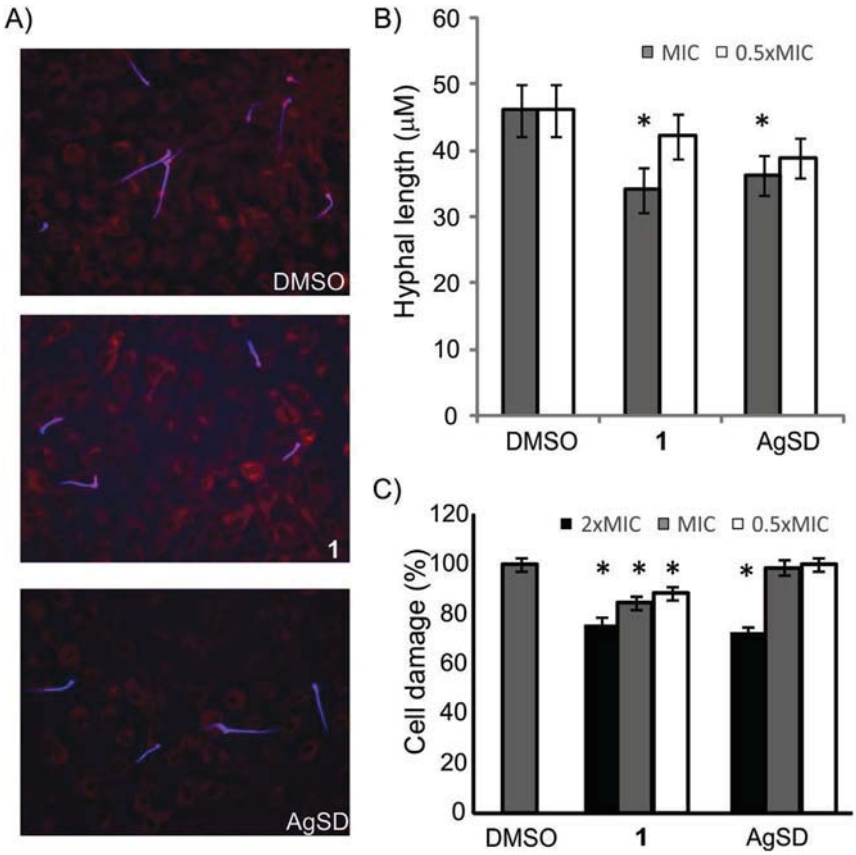

Fig. 2. The effect of **1** and AgSD on *C. albicans* SC5314 virulence in epithelial infection model. (A) Invasion (100 × magnification), (B) hyphal length and (C) % cell damage in comparison to DMSO treated cells (*P < 0.5, Student t-test).

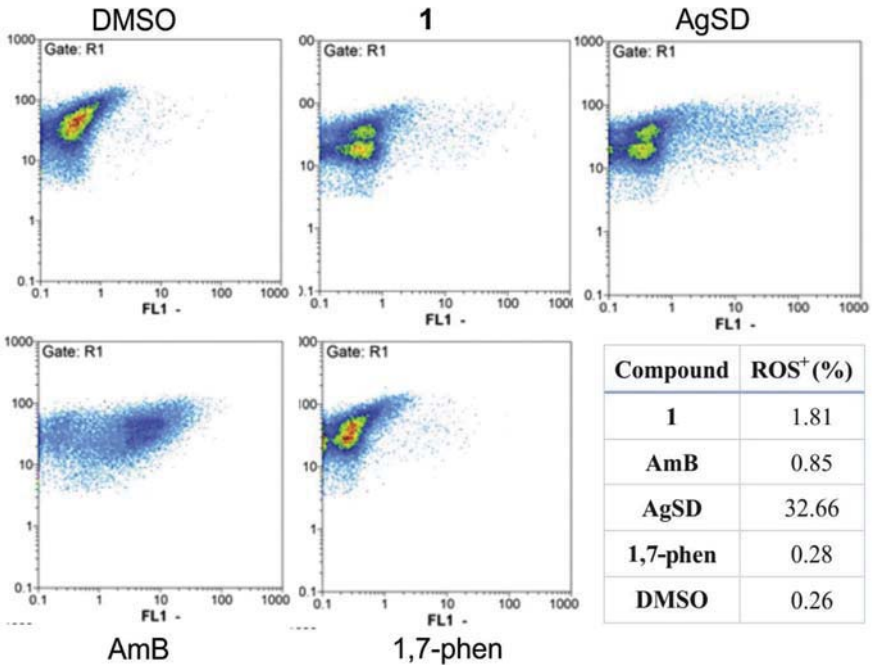

Compound	ROS^{+}(%)
1	1.81
AmB	0.85
AgSD	32.66
1,7-phen	0.28
DMSO	0.26

Fig. 3. Reactive oxygen species (ROS) generation in *C. albicans* cells treated with 2-fold MIC concentrations of silver(I) complex **1**, 1,7-phenanthroline (1,7-phen), AgSD and AmB (amphotericin B) for 1.5 h. ROS were detected using 2′,7′-dichlorofluorescin diacetate (DCFH-DA) staining with cells treated with DMSO used as a control.

new drug compounds design strategies. In most cases, drug binding is non-covalent, although in the case of reactive drugs covalent bonds may be formed [52,53]. Four different modes of drug binding to DNA are known: intercalation of drug between adjacent base pairs, drug binding into the minor groove, binding into the major groove, and backbone tracking binding. For small molecules, the main binding modes are intercalation and minor groove binding [52–54]. Sequence specificity for these binding modes is significantly higher for binding into the minor groove binders than for intercalators [52,54]. The majority of intercalating drugs show preferences to GC-rich sequences and region with alternating G and C bases [54,55]. The intercalation requires conformational changes of the DNA owing to formation of a binding cavity [52,53], which is not required for the minor groove binding. Majority of drugs bonded into the minor groove have a preference of binding to AT-rich sequences [53,56,57]. The major groove offers greater opportunity for forming hydrogen bonds with the drug [52], although the proteins often occupy this groove. The minor groove binding drugs can effect on biological activity of these proteins [54].

Although nucleic acids are more flexible than proteins [58–61], the treatment of DNA as a rigid molecule during docking study does not necessarily lead to worthless results if the sequence DNA base and structure of drug take it into consideration. Namely, the binding of 1,7-phen in AT-rich region of DNA minor groove (Fig. 4A) indicates that the intercalation probably is not an appropriate binding mode to DNA. Also, in accordance with the tendency of complex **1** to bind into the minor groove in the AT-rich region (Fig. 4A), it may be expected that the intercalation of this complex is not an appropriate binding mode to DNA. However, by visual analysis of crystal structures from Protein Data Bank, we found that metal complexes with aromatic ligands intercalate between adjacent base pairs. On the other hand, Monte Carlo simulations showed that there is a possible migration from AT-rich region into the minor groove to site between adjacent base pairs, and achieved that van der Waals interactions are the driving force for this migration [62]. In accordance with the results of visual analysis and MC simulations, we can presume that the intercalation probably is an appropriate binding mode to DNA for complex **1**. Despite stronger binding of complex **1** into the minor groove of DNA (−7.06 kcal/mol) than 1,7-phen (−3.83 kcal/mol), the nature of its interactions with DNA is in favor of the previous presumption. Namely, both examined compounds form only weak non-covalent interactions with a DNA (weak hydrogen bonds, van der Waals interaction and interactions of π-system). Complex **1** has only two rotatable bonds (Ag—N coordination bonds) as internal degrees of freedom, that allow the conformation of the complex in which the one 1,7-phen ligand is intercalated between the base pairs, and the other one is bonded into the minor groove in the AT-rich region. The intercalation of the second 1,7-phen ligand is conformationally restricted, because of the coordination (N—Ag—N) angle strain. *In vitro* DNA interaction evaluation by gel electrophoresis, revealed that under the tested conditions neither **1** nor 1,7-phen were able to interact with *C. albicans* double stranded genomic DNA in a way to prevent ethidium bromide binding and they were not causing DNA degradation (Fig. 4B). This is in contrast to 1,10-phendio and $[Ag(1,10\text{-phendio})_2]ClO_4$ that caused extensive and non-specific DNA cleavage [17,18]. Furthermore, circular dichroism (CD) spectroscopy has also been used as a useful technique for analyzing interactions between the metal complexes and DNA, and it is also very sensitive to the mode of DNA interaction with small molecules [63]. The CD spectrum of double-stranded template DNA (dsDNA) isolated from herring sperm exhibits a positive band at 277 nm due to base stacking interactions and a negative band at 245 nm due to helicity and is characteristic of DNA in right-handed B form [64]. It is well known that intercalation tends to enhance the intensities of both bands due to strong base stacking interactions and stable DNA conformations. On the other side, simple groove binding and electrostatic interactions with small molecules show less or no perturbation on the base-stacking and helicity bands. In the presence of the complex **1** at relatively high concentration of 400 μM, an increase in intensity of the positive band and decrease in intensity of the negative band of DNA have been observed (Fig. 4C). In

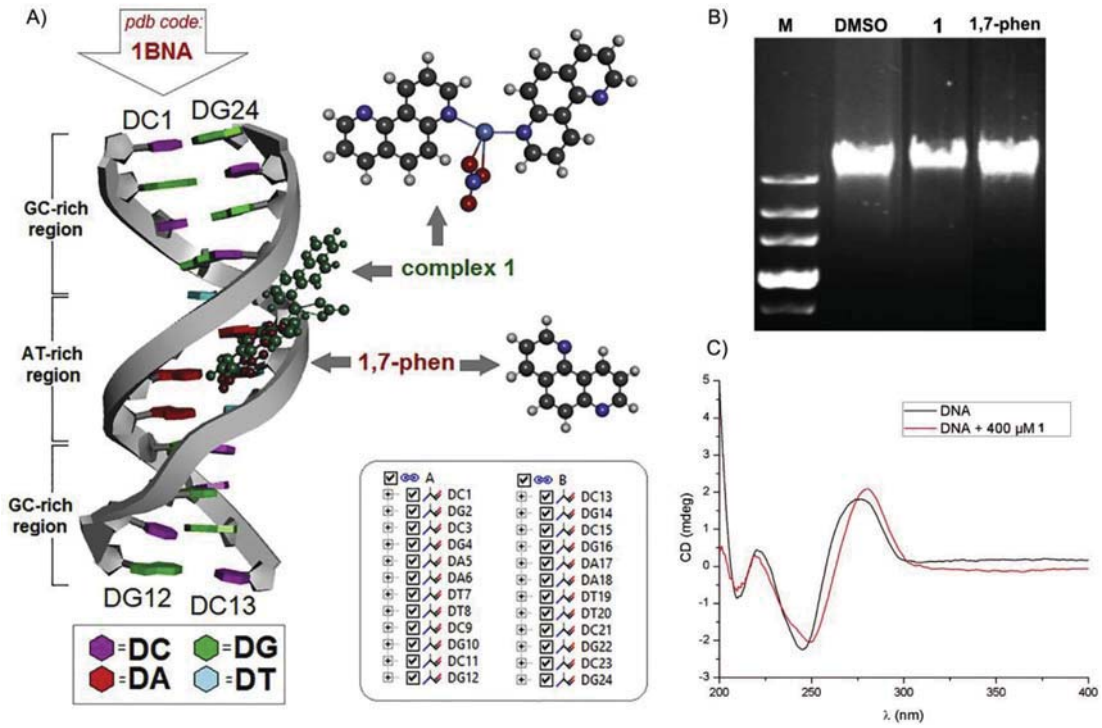

Fig. 4. *In vitro* interaction of silver(I) complex **1** with DNA. (A) The structures of DNA (pdb code-1BNA), complex **1** and 1,7-phen and the most stable binding of the investigated compounds to DNA, as assessed by molecular docking. (B) *In vitro* interaction with *C. albicans* chromosomal DNA assessed by gel electrophoresis (100 ng/μL DNA treated with 25 μM compounds for 2 h in 10 mM Tris-Cl, pH 8.5) and (C) CD spectra of DNA (1 mg/mL) treated with complex **1** (400 μM).

addition, this complex showed a red-shift in the positive and negative bands, suggesting conformational change of a B-form DNA to A-form DNA caused by interaction between DNA molecule and the complex. Similar result was observed for [Ag(2,9-dimethyl-1,10-phenanthroline)$_2$]$NO_3 \cdot H_2O$ complex bound to DNA [65].

Most of 'DNA drugs' are generally positively charged aromatic compounds [52]. Thus, [Ag(1,10-phen)$_2$]NO_3 complex has both properties and binds into the minor groove in the GC-rich region (Fig. S4). This complex has a lower binding energy (−4.80 kcal/mol) than complex **1** (−7.06 kcal/mol), and weak non-covalent interactions between complex and DNA are responsible for its binding into the minor groove. However, it is known that the [Ag(1,10-phen)$_2$]NO_3 complex interacts with DNA by intercalating one of the phenanthroline ligands into a DNA helix [66]. Although the complex **1** has a slightly higher affinity for binding to the DNA, these two complexes bind to different regions, therefore, their binding into the minor groove is unimpeded.

Overall, DNA may not be the primary target of **1** within *Candida* cells, however it may be one of the biomolecules that this silver(I) complex interacts with.

2.4. Toxicity and therapeutic safety assessment of *1* in zebrafish embryos

Zebrafish has been suggested as suitable animal model for *in vivo* drug discovery and development [67], and has been successfully utilized for the safety assessment of metal complexes with biomedical application [25,28]. Therefore, the toxicity of the complex **1** was investigated using the 6 hpf zebrafish (*Danio rerio*) embryos in a 114 h exposure study and compared with the toxicity of the 1,7-phen and AgSD as a clinically used antimicrobial agent. The results obtained in this study showed that both **1** and 1,7-phen were less toxic (lethal and teratogenic) than AgSD (Fig. 5A). These results of the toxicity *in vivo* are in agreement with the results obtained on the human fibroblast (MRC5) cells (Table 1).

Based on the determined LC_{50} values, **1** was slightly (1.2-fold) less toxic to zebrafish embryos than AgSD and 7.8-fold more toxic than 1,7-phen. All embryos exposed to 10 μM of **1** showed possible small pericardial edemas and a few of them had slightly reduced head (Fig. 5B). Complex **1** elicited no toxic response (lethal nor teratogenic) in zebrafish embryos upon treatment with doses close to anti-*C. albicans* and *C. parapsilosis* MIC values (Table 1), indicating favorable therapeutic profile of this complex. The LC_{50} values of 1,7-phen are in line with our recently published results [25].

With the aim to compare the therapeutic potential of **1** to that of AgSD, we determined their therapeutic index (Ti) and the therapeutic safety index (Ts) (Table 2). AgSD appeared more toxic (teratogenic) than **1** and exerted side effects at the doses bellow its anti-*Candida* MIC values, such as developmental abnormalities already at 1 μM and the cardiotoxicity at ≥ 2.5 μM demonstrating low therapeutic safety (Table 2). To the best of our knowledge this is the first study exploring a dose-dependent toxicity of AgSD in the zebrafish model.

It is also important to note that **1** did not affect cardiovascular functions of zebrafish embryos in constrast to AgSD (Fig. S5). Numerous studies highlighted cardiac toxicity (cardiomyopathy, arrhythmias, cardiac enlargement and failure) in patients receiving some antifungal drugs, such as azoles (ketonazole, itraconazole and fluconazole), echinocandins, and especially amphotericin B and its derivatives [68–70]. Therefore, development of novel antifungals without inherent cardiotoxic implications is critical.

Based on therapeutic index, it can be concluded that complex **1** present novel antifungal compound with much higher therapeutic potential and safety profile than silver(I) sulfadiazine, what together with a spectrum of its antifungal activities makes this complex as an excellent candidate for further application to combat

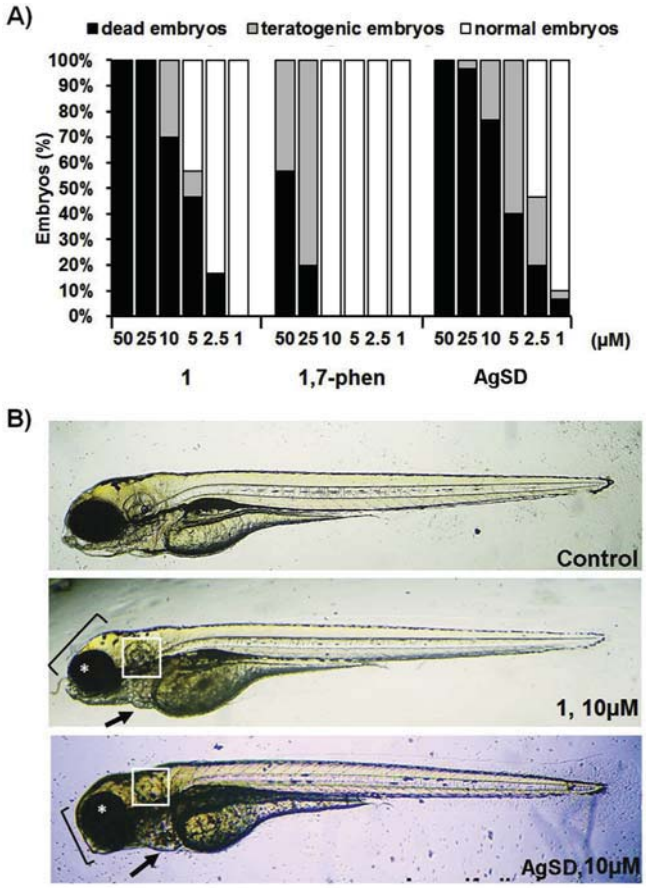

Fig. 5. Toxicity assessment of silver(I) complex **1**, 1,7-phen and silver(I) sulfadiazine (AgSD) in zebrafish embryos exposed to different concentrations (1–50 μM) (A). Morphology of zebrafish embryos at 114 hpf upon different treatments (B). Embryos exposed to 10 μM of **1** (slightly affected), and AgSD (severely malformed) are shown. Malformed head (bracket), reduced eyes (asterisk) and otoliths (boxed) size, large pericardial edema (arrow).

Table 2
Evaluation of the therapeutic index (Ti) and the therapeutic safety index (Ts) of **1** in comparison to silver(I) sulfadiazine (AgSD).

Compound	MIC (μM)	LC_{50} (μM)	EC_{50} (μM)	Ti	Ts
1	1.8	5.89	4.13	3.27	2.29
AgSD	10	5.02	2.23	0.50	0.22

MIC – the minimal inhibitory concentration determined against *C. albicans*.
LC_{50} – the concentration causing lethal effect at 50% zebrafish embryos.
EC_{50} – the concentration inducing side effects (lethality and teratogenicity) at 50% embryos.
Ti – the therapeutic index determined as the ratio between LC_{50} value and MIC value.
Ts – the therapeutic safety index determined as the ratio between EC_{50} value and MIC value.

candidal infections.

*2.4.1. Oxidative stress in zebrafish embryos upon exposure to **1***

It is well known that the long-term application of some commercial antifungals, like amphotericin B, is limited due to the toxicity towards human kidney cells associated with generation of oxidative stress [71,72], as well as towards normal human dermal fibroblasts [73]. Therefore, an evaluation of novel antifungal agents for the potential to provoke oxidative stress *in vivo* and inflict the oxidative stress-mediated damages is of great importance for their further medical application.

Assessment of ROS production performed in this study using the zebrafish model revealed significant differences in the oxidative stress response between embryos exposed to **1** and AgSD (Fig. 6). These differences became visible already at the doses corresponding to the MIC values, at which **1** generated markedly less ROS than AgSD ($P < 0.05$, Student t-test; Fig. 6A). Moreover, the ROS level measured in embryos upon the MIC doses of **1** did not differ significantly from the basal level detected in the control group ($P \geq 0.05$; Student t-test), while AgSD treatment significantly increased embryos' ROS at the MIC dose, accounting for 127% compared to the control group ($P \geq 0.05$, Student t-test; Fig. 6B).

It is noteworthy that complex **1,** exhibiting the best antifungal activity (Table 1) and therapeutic potential (Table 2), did not elevate the ROS production in zebrafish embryos even at the 5 × MIC dose (data not shown) neither caused developmental abnormalities, demonstrating thus a very good overall toxicity profile. Only at a dose of the 6 × MIC value, **1** weakly increased the oxidative stress in exposed embryos (up to 111 ± 4%; Fig. 6B), mostly manifested as a visible fluorescence of pericardial sac (Fig. 6A), while not disturbing normal heartbeat rate. On the other side, AgSD-treated embryos displayed intensive fluorescence over the whole body and cardiotoxic side effects (pericardial sac fluorescence accompanied with pericardial edema) already upon a dose corresponding to the MIC value, additionally confirming their low therapeutic safety *in vivo*. Such side effects were particularly pronounced at a 4 × MIC dose (Fig. 6B). Previous studies performed in the zebrafish model evidenced oxidative stress as one of the mechanisms of silver-based compounds' toxicity, whereas cardiotoxicity has been frequently reported as the toxic effect caused by Ag^+ ions [74,75]. Absence of cardiotoxicity and detectable oxidative stress in the zebrafish model during the treatments with **1** at antifungal doses (≥MIC) demonstrates better pharmacological properties of this phenanthroline-based silver(I) complex in comparison to the clinically used antifungals.

3. Conclusion

In the present research study, five novel silver(I) complexes with 1,7-phenanthroline as ligand (**1**–**5**) were synthesized, structurally characterized and biologically evaluated. The spectroscopic and crystallographic results revealed that all synthesized silver(I) complexes are mononuclear species with the metal ion being monodentatedly coordinated by two ligand molecules *via* less sterically hindered N7 nitrogen. These complexes showed selectivity towards *Candida* spp. in comparison to bacteria, being moderately cytotoxic against healthy human fibroblasts. Complex **1**, which showed the best therapeutic potential, attenuated *C. albicans* virulence and reduced epithelial cell damage in the cell infection model. Moreover, this complex induced the ROS response in *C. albicans*, with fungal DNA being one of the possible target biomolecules. Besides that, *in vivo* assessment performed on the zebrafish embryos showed that this complex was less toxic than silver(I) sulfadiazine, which is the clinically used antimicrobial, without affecting cardiovascular functions and elevating the ROS production in the zebrafish embryos. Taken all these together, silver(I) complex **1** may present novel potent antifungal compound with favorable pharmacological properties, being more effective and safe than the clinically used silver(I) sulfadiazine.

4. Experimental section

4.1. Materials

Distilled water was demineralized and purified to a resistance of

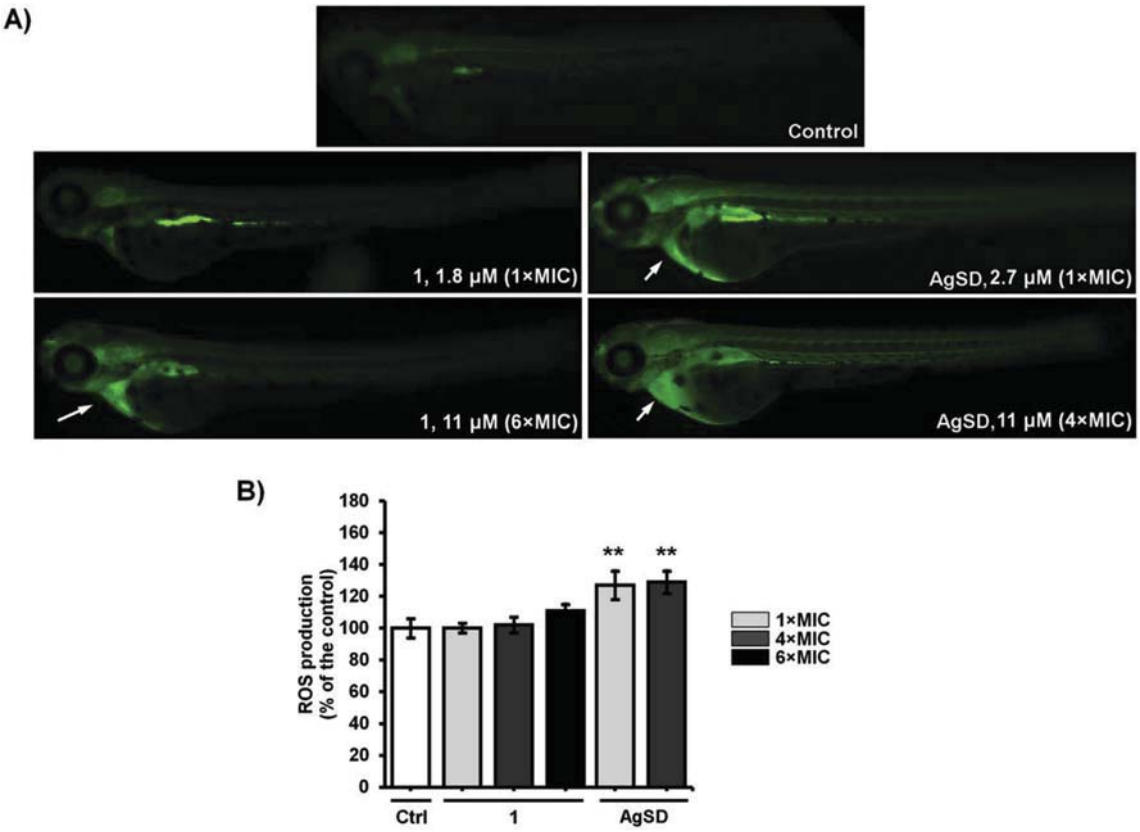

Fig. 6. Reactive oxygen species (ROS) production in zebrafish embryos exposed to different doses (1 × MIC, 4 × MIC and 6 × MIC) of **1** and AgSD. A) ROS levels were determined by measuring the fluorescence of individual zebrafish embryos. B) Statistically significant differences between data of untreated control and treatments were denoted with asterisk (*P < 0.5, **P < 0.01; ***P < 0.001; Student t' test).

greater than 10 MΩ cm. The starting silver(I) salts ($AgNO_3$, $AgClO_4$, $AgCF_3SO_3$, $AgBF_4$ and $AgSbF_6$), 1,7-phenanthroline (1,7-phen), methanol, ethanol, acetone, acetonitrile, dimethyl sulfoxide (DMSO), dimethylformamide (DMF), deuterated dimethylformamide (DMF-d_7) and dimethyl sulfoxide (DMSO-d_6) were purchased from Sigma-Aldrich. All the employed chemicals were of analytical reagent grade and used without further purification.

4.2. Measurements

Elemental microanalyses of the synthesized silver(I) complexes for carbon, hydrogen and nitrogen were performed by the Microanalytical Laboratory, Faculty of Chemistry, University of Belgrade and Adolphe Merkle Institute, University of Fribourg. All NMR spectra were recorded at 25 °C on a Bruker Avance III 400 MHz spectrometer (^{1}H at 400 MHz, ^{13}C at 101 MHz). 5 mg of each compound was dissolved in 0.6 mL of DMF-d_7 and transferred into a 5 mm NMR tube. Chemical shifts are reported in ppm (δ) and scalar couplings are reported in Hertz. In order to investigate the solution behavior of silver(I) complexes, the ^{1}H NMR spectra were recorded immediately after their dissolution in DMSO-d_6 (DMSO is a solvent used for biological evaluation of the complexes), as well as after 48 h standing in the dark at room temperature. The IR spectra were recorded as KBr pellets on a Perkin Elmer Spectrum 100 spectrometer over the wavenumber range of 4000−450 cm^{-1}. The ESI-MS spectra in positive mode were recorded after dissolving the silver(I) complexes **1**−**5** in DMF/H_2O (1: 9, v/v) mixture with a Bruker Esquire Ion Trap mass spectrometer. The UV−Vis spectra were recorded over the wavelength range of 900−200 nm on a Shimadzu double-beam spectrophotometer after dissolving the silver(I) complexes **1**−**5** in DMF/H_2O (1: 9, v/v). The concentration of the silver(I) complexes was $1.3{\cdot}10^{-5}$ M.

4.3. Synthesis of silver(I) complexes

4.3.1. Synthesis of *1*

Silver(I) complex [Ag(NO_3-*O,O'*) (1,7-phen-*N7*)$_2$] (**1**) was synthesized according to the modified procedure for the preparation of silver(I) complexes with phthalazine and quinazoline [26]. The solution of 1.0 mmol of $AgNO_3$ (169.9 mg of $AgNO_3$) in 15 mL of warm methanol was added slowly under stirring to the solution containing 0.5 mmol (90.1 mg) of 1,7-phen, dissolved in 15 mL of warm acetone. The reaction mixture was stirred in the dark at room temperature for 3 h. A white precipitate, which was formed after evaporation of the mother solution at room temperature, was filtered off and dissolved in acetonitrile. The obtained solution was left to slowly evaporate at room temperature to a volume of 5.0 mL, and then stored in a refrigerator at +4 °C. After two days colorless crystals of **1**, suitable for single crystal X-ray crystallography were formed. Yield (calculated on the basis of *N*-heterocyclic ligand): 100.8 mg (76%).

Anal. calcd. for **1** = $C_{24}H_{16}AgN_5O_3$ (MW = 530.29): C, 54.36; H, 3.04; N, 13.21. Found: C, 53.95; H, 2.92; N, 13.37%. ^{1}H NMR (400 MHz, DMF-d_7): δ = 8.02 (*dd*, *J* = 8.1, 4.4 Hz, H4), 8.13 (*dd*, *J* = 8.3, 4.6 Hz, H10), 8.42 (*d*, *J* = 9.1 Hz, H3), 8.46 (*d*, *J* = 9.1 Hz, H9), 8.79 (*dd*, *J* = 8.1, 1.7 Hz, H5), 9.34 (*dd*, *J* = 4.4, 1.7 Hz, H2), 9.42 (*dd*, *J* = 4.5, 1.7 Hz, H8), 9.88 ppm (*dd*, *J* = 8.3, 1.7 Hz, H6). ^{13}C NMR (101 MHz, DMF-d_7): δ = 122.85 (C10), 123.47 (C4), 126.54 (C4a), 127.32 (C10a), 128.89 (C3), 130.33 (C9), 133.31 (C6), 136.68 (C5), 145.53 (C1a), 149.16 (C6a), 150.48 (C2), 152.72 ppm (C8). IR (KBr, ν,

cm^{-1}): ~3040w, 2921w ($\nu(C_{ar}-H)$), 1617w, 1599 m, 1573w, 1496 m ($\nu(C_{ar}=C_{ar})$ and $\nu(C_{ar}=N)$), 1384vs and 1297s ($\nu_{as}(NO_3)$), 836s, 773s ($\gamma(C_{ar}-H)$), 726w and 700w ($\delta(NO_3)$). UV–Vis (DMF/H_2O, λ_{max}, nm): 268.0 ($\varepsilon = 4.1{\cdot}10^4\ M^{-1}cm^{-1}$). (+)ESI-MS (DMF/$H_2O$) *m/z* (relative intensity): 468.0 $[Ag(1,7\text{-phen})_2]^+$ (100), 361.0 $[Ag(1,7\text{-phen})\ (DMF)]^+$ (10).

*4.3.2. Synthesis of **2**–**5***

Silver(I) complexes [Ag(1,7-phen-*N7*)$_2$]X, X = ClO_4^- (**2**), $CF_3SO_3^-$ (**3**), BF_4^- (**4**) and SbF_6^- (**5**) were synthesized according to the modified procedure for the preparation of silver(I) complexes with phthalazine, quinazoline and 2,3-diphenylquinoxaline [27,76]. The solution of 1.0 mmol of the corresponding silver(I) salt (207.3 mg of $AgClO_4$ for **2**, 256.9 mg of $AgCF_3SO_3$ for **3**, 194.7 mg of $AgBF_4$ for **4** and 343.6 mg of $AgSbF_6$ for **5**) in 5.0 mL of ethanol was added slowly under stirring to the solution containing an equimolar amount of 1,7-phen (180.2 mg) in 20.0 mL of warm ethanol. The reaction mixture was stirred in the dark at room temperature for 3 h. The solid products of complexes **2** and **5** precipitated during this time or after evaporation of the mother solution at room temperature, respectively, were filtered off and dried in the dark at ambient temperature. Our attempts to obtain the crystals suitable for X-ray analysis for these complexes from their amorphous powders using different solvents were unsuccessful. However, complexes **3** and **4** were crystallized from mother ethanol solution after its standing at room temperature for several days. Yield (calculated on the basis of the *N*-heterocyclic ligand): 193.0 mg (68%) for **2**, 222.2 mg (72%) for **3**, 177.6 mg (64%) for **4** and 183.4 mg (52%) for **5**.

Anal. calcd. for **2** = $C_{24}H_{16}AgClN_4O_4$ (MW = 567.73): C, 50.77; H, 2.84; N, 9.87. Found: C, 51.17; H, 2.70; N, 9.31%. ^{1}H NMR (400 MHz, DMF-d_7): δ = 8.01 (*dd*, *J* = 8.1, 4.4 Hz, H4), 8.10 (*dd*, *J* = 8.3, 4.5 Hz, H10), 8.40 (*d*, *J* = 9.1 Hz, H3), 8.47 (*d*, *J* = 9.1 Hz, H9), 8.78 (*dd*, *J* = 8.1, 1.7 Hz, H5), 9.33 (*dd*, *J* = 4.4, 1.7 Hz, H2), 9.39 (*dd*, *J* = 4.5, 1.7 Hz, H8), 9.85 ppm (*ddd*, *J* = 8.3, 1.7, 0.7 Hz, H6). ^{13}C NMR (101 MHz, DMF-d_7): δ = 122.85 (C10), 123.47 (C4), 126.54 (C4a), 127.31 (C10a), 128.89 (C3), 130.31 (C9), 133.29 (C6), 136.68 (C5), 145.49 (C1a), 149.20 (C6a), 150.48 (C2), 152.69 ppm (C8). IR (KBr, ν, cm^{-1}): ~3048w, 2923w ($\nu(C_{ar}-H)$), 1617w, 1600 m, 1575w, 1497 m ($\nu(C_{ar}=C_{ar})$ and $\nu(C_{ar}=N)$), 1108vs and 1064s ($\nu(ClO_4)$), 833s, 775s ($\gamma(C_{ar}-H)$), 622s (δ(OClO)). UV–Vis (DMF/H_2O, λ_{max}, nm): 269.0 ($\varepsilon = 5.1{\cdot}10^4\ M^{-1}cm^{-1}$). (+)ESI-MS (DMF/$H_2O$) *m/z* (relative intensity): 468.0 $[Ag(1,7\text{-phen})_2]^+$ (100), 361.0 $[Ag(1,7\text{-phen})\ (DMF)]^+$ (3).

Anal. calcd. for **3** = $C_{25}H_{16}AgF_3N_4O_3S$ (MW = 617.35): C, 48.64; H, 2.61; N, 9.08. Found: C, 48.92; H, 2.54; N, 8.89%. ^{1}H NMR (400 MHz, DMF-d_7): δ = 8.02 (*dd*, *J* = 8.3, 4.5 Hz, H4), 8.11 (*dd*, *J* = 8.3, 4.5 Hz, H10), 8.41 (*d*, *J* = 9.1 Hz, H3), 8.48 (*d*, *J* = 9.1 Hz, H9), 8.79 (*dd*, *J* = 8.1, 1.7 Hz, H5), 9.34 (*dd*, *J* = 4.4, 1.7 Hz, H2), 9.40 (*dd*, *J* = 4.5, 1.8 Hz, H8), 9.86 ppm (*ddd*, *J* = 8.3, 1.7, 0.7 Hz, H6). ^{13}C NMR (101 MHz, DMF-d_7): δ = 122.88 (C10), 123.50 (C4), 126.55 (C4a), 127.35 (C10a), 128.88 (C3), 130.38 (C9), 133.39 (C6), 136.69 (C5), 145.53 (C1a), 149.15 (C6a), 150.51 (C2), 152.79 ppm (C8). IR (KBr, ν, cm^{-1}): ~3047w, 2923w ($\nu(C_{ar}-H)$), 1616w, 1602 m, 1575w, 1499 m ($\nu(C_{ar}=C_{ar})$ and $\nu(C_{ar}=N)$), 1286vs ($\nu_{as}(SO_3)$), 1247vs ($\nu_s(CF_3)$), 1155s ($\nu_{as}(CF_3)$), 1027s ($\nu_s(SO_3)$), 835s, 771s ($\gamma(C_{ar}-H)$), 754 m ($\delta_s(CF_3)$), 637 m ($\delta_s(SO_3)$), 594 m ($\delta_{as}(CF_3)$), 516 m ($\delta_{as}(SO_3)$). UV–Vis (DMF/H_2O, λ_{max}, nm): 269.0 ($\varepsilon = 4.1{\cdot}10^4\ M^{-1}cm^{-1}$). (+)ESI-MS (DMF/$H_2O$) *m/z* (relative intensity): 468.0 $[Ag(1,7\text{-phen})_2]^+$ (100), 361.0 $[Ag(1,7\text{-phen})\ (DMF)]^+$ (17).

Anal. calcd. for **4** = $C_{24}H_{16}AgBF_4N_4$ (MW = 555.09): C, 51.93; H, 2.91; N, 10.09. Found: C, 51.87; H, 2.79; N, 10.10%. ^{1}H NMR (400 MHz, DMF-d_7): δ = 8.01 (*dd*, *J* = 8.0, 4.3 Hz, H4), 8.09 (*dd*, *J* = 8.2, 4.5 Hz, H10), 8.38 (*d*, *J* = 9.0 Hz, H3), 8.46 (*d*, *J* = 9.1 Hz, H9), 8.78 (*d*, *J* = 8.1 Hz, H5), 9.33 (*d*, *J* = 4.3 Hz, H2), 9.37 (*d*, *J* = 4.3 Hz, H8), 9.84 ppm (*d*, *J* = 8.3 Hz, H6). ^{13}C NMR (101 MHz, DMF-d_7): δ = 122.79 (C10), 123.42 (C4), 126.53 (C4a), 127.20 (C10a), 128.91 (C3), 130.15 (C9), 133.11 (C6), 136.66 (C5), 145.56 (C1a), 149.26 (C6a), 150.43 (C2), 152.53 ppm (C8). IR (KBr, ν, cm^{-1}): ~3078w, 2963w ($\nu(C_{ar}-H)$), 1617w, 1600 m, 1575w, 1498 m ($\nu(C_{ar}=C_{ar})$ and $\nu(C_{ar}=N)$), 1059vs ($\nu_{as}(BF_4)$), 832s, 774s ($\gamma(C_{ar}-H)$), 793 m ($\nu_s(BF_4)$). UV–Vis (DMF/H_2O, λ_{max}, nm): 269.0 ($\varepsilon = 5.3{\cdot}10^4\ M^{-1}cm^{-1}$). (+)ESI-MS (DMF/$H_2O$) *m/z* (relative intensity): 468.0 $[Ag(1,7\text{-phen})_2]^+$ (100), 361.0 $[Ag(1,7\text{-phen})\ (DMF)]^+$ (5).

Anal. calcd. for **5** = $C_{24}H_{16}AgF_6N_4Sb$ (MW = 704.03): C, 40.94; H, 2.29; N, 7.96. Found: C, 40.78; H, 2.15; N, 7.68%. ^{1}H NMR (400 MHz, DMF-d_7): δ = 8.02 (*dd*, *J* = 8.1, 4.4 Hz, H4), 8.13 (*dd*, *J* = 8.3, 4.6 Hz, H10), 8.47 (*m*, H3 and H9, isochronous), 8.78 (*dd*, *J* = 8.1, 1.7 Hz, H5), 9.34 (*dd*, *J* = 4.4, 1.7 Hz, H2), 9.44 (*dd*, *J* = 4.6, 1.7 Hz, H8), 9.88 ppm (*dd*, *J* = 8.3, 1.6 Hz, H6). ^{13}C NMR (101 MHz, DMF-d_7): δ = 122.97 (C10), 123.58 (C4), 126.56 (C4a), 127.48 (C10a), 128.85 (C3), 130.60 (C9), 133.73 (C6), 136.72 (C5), 145.42 (C1a), 148.92 (C6a), 150.59 (C2), 153.13 ppm (C8). IR (KBr, ν, cm^{-1}): ~3082w, 2949w ($\nu(C_{ar}-H)$), 1619w, 1600 m, 1575w, 1497 m ($\nu(C_{ar}=C_{ar})$ and $\nu(C_{ar}=N)$), 836s, 778s ($\gamma(C_{ar}-H)$), 656vs ($\nu(SbF_6)$). UV–Vis (DMF/H_2O, λ_{max}, nm): 269.0 ($\varepsilon = 5.4{\cdot}10^4\ M^{-1}cm^{-1}$). (+)ESI-MS (DMF/$H_2O$) *m/z* (relative intensity): 468.0 $[Ag(1,7\text{-phen})_2]^+$ (100), 361.0 $[Ag(1,7\text{-phen})\ (DMF)]^+$ (14).

1,7-phen data given for comparative purposes. MW = 180.21. ^{1}H NMR (400 MHz, DMF-d_7): δ = 7.98 (*m*, H4 and H10), 8.33 (*dd*, *J* = 53.8, 9.1 Hz, H3 and H9), 8.74 (*dd*, *J* = 8.1, 1.7 Hz, H5), 9.29 (*dd*, *J* = 4.3, 1.6 Hz, H2 and H8), 9.75 ppm (*ddd*, *J* = 8.3, 1.8, 0.7 Hz, H6). ^{13}C NMR (101 MHz, DMF-d_7): δ = 122.51 (C10), 123.17 (C4), 126.47 (C4a), 126.87 (C10a), 129.02 (C3), 129.65 (C9), 132.27 (C6), 136.55 (C5), 145.81 (C1a), 149.74 (C6a), 150.16 (C2), 151.78 ppm (C8). IR (KBr, ν, cm^{-1}): 3032w, 2928w ($\nu(C_{ar}-H)$), 1614 m, 1584 m, 1568 m, 1490s, 1426s ($\nu(C_{ar}=C_{ar})$ and $\nu(C_{ar}=N)$), 846vs, 774vs ($\gamma(C_{ar}-H)$). UV–Vis (DMF/H_2O, λ_{max}, nm): 267.0 ($\varepsilon = 2.7{\cdot}10^4\ M^{-1}cm^{-1}$).

4.4. Air/light stability

The air/light stability of **1**–**5** was studied in direct light in air atmosphere at room temperature in order to mimic their exposure to light under real life conditions. Sterile cellulose discs were impregnated with the silver(I) compounds (5 μL of 50 mg/mL DMSO stock solution) and exposed to air and light. The stability was monitored visually within 48 h.

4.5. Crystallographic data collection and refinement of the structures

Single crystals of **1**, **3** and **4** were selected and mounted on a loop with inert oil on a Stoe IPDS2 diffractometer. The crystals were kept at 298(2) K (**1** and **3**) or 250(2) K (**4**) during data collection. Using Olex2 [77], the structure was solved with the ShelXT [78] structure solution program using Intrinsic Phasing and refined with the ShelXL [79] refinement package using Least Squares minimization. Hydrogen atom positions were calculated geometrically and refined using the riding model. Crystal data and details of the structure determinations are listed in Table S2. MERCURY computer graphics program [80] was used to prepare drawings.

4.6. Antimicrobial activity

4.6.1. Antibacterial activity

The minimal inhibitory concentrations (MICs) of the silver(I) complexes **1**–**5**, 1,7-phenanthroline and silver(I) sulfadiazine (AgSD; Sigma, Munich, Germany) against a panel of five microorganisms that included *Escherichia coli* NCTC 9001, *Staphylococcus*

aureus ATCC 25923, *Enterococcus faecalis* ATCC 29212, *Klebsiella pneumoniae* ATCC 13883 and *Pseudomonas aeruginosa* ATCC 27853, were determined according to the standard broth microdilution assay, recommended by the American National Committee for Clinical Laboratory Standards (M07-A8). The tested compounds were dissolved in DMSO. The highest concentration tested was 500 μg/mL and the inoculums were 10^5 colony-forming units (cfu/mL). The MIC value corresponds to the lowest concentration that inhibited the growth after 24 h at 37 °C.

4.6.2. Anti-Candida activity

The minimal inhibitory concentrations (MICs) of the silver(I) complexes **1**–**5**, 1,7-phenanthroline and AgSD against *C. albicans* ATCC 10231, *C. parapsilosis* ATCC 22019, *C. glabrata* ATCC 2001 and *C. krusei* ATCC 6258 were determined in RPMI 1640 medium (Gibco) according to Standards of European Committee on Antimicrobial Susceptibility Testing (v 7.3.1: Method for the determination of broth dilution minimum inhibitory concentrations of antifungal agents for yeasts). The tested compounds were dissolved in DMSO. The highest concentration tested was 500 μg/mL and the inoculums were 10^5 cfu/mL. The MIC value corresponds to the lowest concentration that inhibited the growth after 24 h at 37 °C.

4.6.3. Epithelial cells infection model

The ability of *C. albicans* SC5314 cells to infect epithelial cells TR146 (obtained from Cancer Research Technology, London) was tested in the presence of **1** and silver(I) sulfadiazine (AgSD) in the concentration range of 2 – 16 μg/mL (3.77 – 30.17 μM for **1** and 5.60 – 44.80 μM for AgSD**).** *C. albicans* cells were co-incubated with oral epithelial cells for 3 h (hyphal length, invasion assay) and 24 h (damage assay) in serum-free Dulbecco's modified Eagle's medium (DMEM; Gibco) at 37 °C and 5% CO_2 as described in previous publications [81,82]. In the invasion assay, *C. albicans* cells were first stained with the Alexa Fluor 488 conjugate of succinylated concanavalin A (ConA; Invitrogen). Afterwards, epithelial cells were permeabilized using 0.5% Triton X-100 and fungal cells stained with calcofluor-white (CFW; Sigma), which allowed differentiation of invading (stained by CFW only) and non-invading (stained by both CFW and ConA) hyphae. Using fluorescence microscopy, the percentage of invading cells and hyphal length were determined by counting at least 50 invading *Candida* cells. Epithelial cell damage was determined after 24 h by measuring the release of lactate dehydrogenase (LDH) using the LDH cytotoxicity detection kit (Roche Applied Science) according to manufacturer instructions. All experiments were performed in triplicates for each condition and repeated three times.

4.6.4. Measurement of ROS production in Candida

Intracellular reactive oxygen species (ROS) were measured using the fluorescent dye 2′,7′-dichlorofluorescin diacetate (DCFH-DA, Sigma) as previously described [83]. Briefly, the *C. albicans* cells were adjusted to 10^7 cells per mL in Sabouraud dextrose broth and incubated for 1.5 h at 30 °C and 200 rpm with 4xMIC concentrations of silver(I) complex **1**, 1,7-phen and silver(I) sulfadiazine. The positive control was treated with 4 μg/mL of amphotericin B. After staining with 10 μM DCFH-DA at 30 °C for 30 min, the cells were collected and washed two times with PBS. The fluorescence intensities (excitation and emission of 488 and 540 nm, respectively) of cells were tested with CyFlow Space Partec flow cytometer with Partec FloMax software (Partec GmbH, Munster, Germany). This experiment was carried out three times independently.

4.7. Cytotoxicity

Cytotoxicity in terms of the antiproliferative effect was tested by the 3-(4,5-dimethylthiazol-2-yl)-2,5-diphenyltetrazolium bromide (MTT) assay [84]. The assay was carried out using human lung fibroblasts (MRC5) cell line after 48 h of cell incubation in the medium, containing compounds at concentrations ranging from 5 to 200 μM. Briefly, MRC5 cells were maintained in RPMI-1640 medium supplemented with 100 μg/mL streptomycin, 100 U/mL penicillin and 10% (v/v) fetal bovine serum (FBS) (Gibco) as a monolayer (1×10^4 cells per well). All cell lines were grown in humidified atmosphere of 95% air and 5% CO_2 at 37 °C. The MTT assay was performed two times in four replicates. The extent of MTT reduction was measured spectrophotometrically at 540 nm using a Tecan Infinite 200 Pro multiplate reader (Tecan Group Ltd., Mannedorf, Switzerland), and the cell survival was expressed as percentage of the control (untreated cells). Cytotoxicity was expressed as the concentration of the compound inhibiting cell growth by 50% (IC_{50}) in comparison to untreated control.

4.8. DNA interaction

4.8.1. Molecular docking

The structures of the tested silver(I) complex **1,** $[Ag(1,10\text{-phen})_2]^+$ complex and 1,7-phenanthroline were optimized by B3LYP method, with 6–31 g** basis set for non-metal atoms and LanL2DZ basis set for silver. Merz–Kollman atomic charges were calculated at same level, according to the scheme *via* the restrained electrostatic potential (RESP) model [85]. Crystal structure of DNA was extracted from Protein Data Bank (pdb code: 1BNA) [86] and used for docking study as target for tested compounds. The structure represents synthetic double stranded dodecamer d(CpGpCpGpApApTpTpCpGpCpG) with more than one complete turn of right-handed B helix and without DNA intercalation gap. The preparation of DNA structure has been carried out using AutoDock 4.2 software program [87] and includes the adding of hydrogen atoms and removing water molecules from crystal structure. In order to generate grid and docking parameter files in AutoDockTools program [87], the optimized structures of the tested compounds and DNA were used. The structure of DNA, $[Ag(1,10\text{-phen})_2]^+$ complex and 1,7-phenanthroline ligand were considered as rigid, while Ag—N coordination bonds of the silver(I) complex **1** were allowed to rotate freely. To accommodate the tested compounds during docking study, a grid box, containing the whole protein, was used. The virtual screening used Lamarckian genetic algorithm as the search method and 100 runs for each docking screen. Discovery Studio (BIOVIA Software product) [88] was used to analyze and visualize the results of docking studies.

4.8.2. In vitro DNA interaction

For DNA interaction assay high molecular weight (HMW) genomic DNA isolated from *C. albicans* ATCC 10231 was used. DNA was isolated according to method of Nikodinovic et al. [89]. DNA (100 ng/μL final concentration) was incubated with 25 μM final concentration of silver(I) complex **1**, 1,7-phen and AgSD in 10 mM Tris-Cl, pH 8.5 in 50 μL reaction volume. After 2 h incubation at 30 °C, 10 μL aliquots were taken, mixed with loading dye and loaded on agarose gel. Control contained an appropriate volume of DMSO. DNA samples were run, 500 ng per lane, on 0.8% agarose gel with ethidium bromide against a O'GeneRuler™ 1 kb Plus DNA Ladder (band sizes in bp: 75, 200, 350, 400, 500, 700, 1000, 1500, 2000, 3000, 4000, 5000, 7000, 10 000, 20 000) (Thermo Scientific™) at 50 V for 3 h. Gels were visualized and analyzed using the Gel Doc EZ system (Bio-Rad, Life Sciences, Hercules, USA), equipped with the Image Lab™ Software.

4.8.3. CD spectral analysis

CD spectra of double-stranded template DNA (dsDNA) from

herring sperm (1 mg/mL; Boehringer Mannheim GmbH, Germany) and its complexes with various amounts of **1** (0–500 μM) were recorded on a Jasco J-815 circular dichroism spectropolarimeter (JASCO, UK) calibrated with ammonium (+)-10-camphorsulfonate. Spectra were recorded over a wavelength range 320–220 nm in 0.1 nm steps at instrument scanning rate of 200 nm/min using a quartz cell of 0.1 mm optical path length and with data integration time of 2 s. The obtained values were normalized by subtracting the baseline recorded for the buffer (10 mM sodium bicarbonate buffer, pH 8.0). The results are expressed as ellipticity, measured in mdeg.

4.9. Embryotoxicity using the zebrafish (Danio rerio) model

Evaluation of toxicity of **1**, 1,7-phen and AgSD on zebrafish embryos model was carried out according to general rules of the OECD Guidelines for the Testing of Chemicals [90]. All experiments involving zebrafish were performed in compliance with the European directive 2010/63/EU and the ethical guidelines of the Guide for Care and Use of Laboratory Animals of the Institute of Molecular Genetics and Genetic Engineering, University of Belgrade.

Adult zebrafish (*Danio rerio*, wild type) were obtained from a commercial supplier (Pet Center, Belgrade, Serbia), housed in a temperature- and light-controlled facility with 28 °C and standard 14:10-h light-dark photoperiod, and regularly fed with commercially dry flake food (TetraMin™ flakes; Tetra Melle, Germany) twice a day and *Artemia nauplii* once daily. Zebrafish embryos were produced by pair-wise mating, collected and distributed into 24-well plates containing 10 embryos per well and 1 mL embryos water (0.2 g/L of Instant Ocean® Salt in distilled water), and raised at 28 °C. For assessing lethal and developmental toxicity, embryos at 6 h post fertilization (hpf) stage were treated with six concentrations of complex **1**, 1,7-phen and AgSD (1, 2.5, 5, 10, 25 and 50 μM). DMSO (0.2%) was used as a negative control. Experiments were performed three times using 20 embryos per concentration.

Apical endpoints for the toxicity evaluation (Table S3) were recorded at 24, 48, 72, 96 and 114 hpf using an inverted microscope (CKX41; Olympus, Tokyo, Japan). Dead embryos were counted and discarded every 24 h. At 114 hpf, embryos were inspected for heartbeat rate, anesthetized by addition of 0.1% (w/v) tricaine solution (Sigma-Aldrich, St. Louis, MO), photographed and killed by freezing at −20 °C for ≥24 h.

4.9.1. Intracellular ROS production in the zebrafish

Generation of intracellular ROS in zebrafish embryos upon **1** and AgSD treatments was detected using an oxidation-sensitive fluorescent probe dye 2′,7′-dichlorofluorescin diacetate (DCFH-DA). Briefly, after 48 h treatment with complex **1**, respective ligand and AgSD, the zebrafish embryos were transferred into 96-well plates, treated with DCFH-DA solution (20 μg/mL) and incubated for 1 h in the dark at 28.5 °C. Following incubation, the zebrafish embryos were rinsed in the fresh embryo water and anesthetized in 0.1% (w/v) tricaine solution (Sigma-Aldrich, St. Louis, MO) before imaging. The images of stained embryos were observed using a fluorescent microscope (Olympus BX51, Applied Imaging Corp., San Jose, CA, USA). A fluorescence intensity of individual zebrafish larvae was measured at an excitation wavelength of 485 nm and an emission wavelength of 535 nm using a spectrofluorometer (Tecan Infinite, 2000 Pro multiplate reader; Tecan Group Ltd., Männedorf, Switzerland).

4.9.2. Statistical analysis

The results were expressed as mean values ± standard deviation (SD) and analyzed using Student's t-test at a threshold level of $P = 0.5$. This analysis was carried out using SPSS 20 (SPSS Inc., Chicago, IL) software.

Ethical statement

All experiments involving zebrafish were performed in compliance with the European directive 2010/63/EU and the ethical guidelines of the Guide for Care and Use of Laboratory Animals of the Institute of Molecular Genetics and Genetic Engineering, University of Belgrade.

Notes

The authors have no competing interests to declare.

Acknowledgments

This research has been financially supported by the Ministry of Education, Science and Technological Development of the Republic of Serbia, under Grants No. 172036 and 173048, the SupraMedChem@Balkans.Net SCOPES Institutional Partnership (Project No. IZ74Z0_160515) and the Serbian Academy of Sciences and Arts (Project No. F128). Work performed in Jena was funded by European Union's Horizon 2020 research and innovation programme under the Marie Sklodowska-Curie Grant Agreement number 642095 (OPATHY) to MP.

Appendix A. Supplementary data

Supplementary data related to this article can be found at https://doi.org/10.1016/j.ejmech.2018.07.049.

References

[1] S.G. Whaley, E.L. Berkow, J.M. Rybak, A.T. Nishimoto, K.S. Barker, P.D. Rogers, Azole antifungal resistance in *Candida albicans* and emerging non-*albicans Candida* species, Front. Microbiol. 7 (2017) 2173.
[2] Q. Saleh, R. Kovács, G. Kardos, R. Gesztelyi, T. Kardos, A. Bozó, L. Majoros, Decreased killing activity of micafungin against *Candida guilliermondii, Candida lusitaniae*, and *Candida kefyr* in the presence of human serum, Microb. Drug Resist. 23 (2017) 764–770.
[3] M.A. Pfallera, P.R. Rhomberg, S.A. Messer, R.N. Jones, M. Castanheira, Isavuconazole, micafungin, and 8 comparator antifungal agents' susceptibility profiles for common and uncommon opportunistic fungi collected in 2013: temporal analysis of antifungal drug resistance using CLSI species-specific clinical breakpoints and proposed epidemiological cutoff values, Diagn. Microbiol. Infect. Dis. 82 (2015) 303–313.
[4] D. Sanglard, F.C. Odds, Resistance of *Candida* species to antifungal agents: molecular mechanisms and clinical consequences, Lancet Infect. Dis. 2 (2002) 73–85.
[5] S.S. Gonçalves, A.C.R. Souza, A. Chowdhary, J.F. Meis, A.L. Colombo, Epidemiology and molecular mechanisms of antifungal resistance in *Candida* and *Aspergillus*, Mycoses 59 (2016) 198–219.
[6] M. Devereux, M. McCann, D.O. Shea, R. Kelly, D. Egan, C. Deegan, K. Kavanagh, V. McKee, G. Finn, Synthesis, antimicrobial activity and chemotherapeutic potential of inorganic derivatives of 2-(4'-thiazolyl)benzimidazole{thiabendazole}: X-ray crystal structures of $[Cu(TBZH)_2Cl]Cl{\cdot}H_2O{\cdot}EtOH$ and $TBZH_2NO_3$ (TBZH = thiabendazole), J. Inorg. Biochem. 98 (2004) 1023–1031.
[7] G. Gasser, N. Metzler-Nolte, The potential of organometallic complexes in medicinal chemistry, Curr. Opin. Chem. Biol. 16 (2012) 84–91.
[8] C. Giulidori, N. Mosconi, B. Toplikar, M. Vega, P. Williams, L. Svetaz, M. Raimondi, M. Rizzotto, Heteroleptic complexes of antifungal drugs with the silver ion, J. Phys. Org. Chem. 29 (2016) 656–664.
[9] K.M. Fromm, Give silver a shine, Nat. Chem. 3 (2011) 178.
[10] R. Rowan, M. McCann, K. Kavanagh, Analysis of the response of *Candida albicans* cells to silver(I), Med. Mycol. 48 (2010) 498–505.
[11] S. Eckhardt, P.S. Brunetto, J. Gagnon, M. Priebe, B. Giese, K.M. Fromm, Nanobio silver: its interactions with peptides and bacteria, and its uses in medicine, Chem. Rev. 113 (2013) 4708–4754.
[12] K. Nomiya, K. Tsuda, T. Sudoh, M. Oda, Ag(I)-N bond-containing compound showing wide spectra in effective antimicrobial activities: polymeric silver(I) imidazolate, J. Inorg. Biochem. 68 (1997) 39–44.
[13] K. Nomiya, S. Takahashi, R. Noguchi, S. Nemoto, T. Takayama, M. Oda, Synthesis and characterization of water-soluble silver(I) complexes with L-histidine (H_2his) and (*S*)-(-)-2-pyrrolidone-5-carboxylic Acid (H_2pyrrld) showing a wide spectrum of effective antibacterial and antifungal activities. Crystal structures of chiral helical polymers $[Ag(Hhis)]_n$ and $\{[Ag(Hpyrrld)]_2\}_n$ in the solid state, Inorg. Chem. 39 (2000) 3301–3311.

[14] M. McCann, M. Geraghty, M. Devereux, D. O'Shea, J. Mason, L. O'Sullivan, Insights into the mode of action of anti-Candida activity of 1,10-phenanthroline and its metal chelates, Met. Base. Drugs 7 (2000) 185–193.

[15] B. Coyle, K. Kavanagh, M. McCann, M. Devereux, M. Geraghty, Mode of antifungal activity of 1,10-phenanthroline and its Cu(II), Mn(II) and Ag(I) complexes, Biometals 16 (2003) 321–329.

[16] B. Coyle, P. Kinsella, M. McCann, M. Devereux, R. O'Connor, K. Kavanagh, Induction of apoptosis in yeast and mammalian cells by exposure to 1,10-phenanthroline metal complexes, Toxicol. Vitro 18 (2004) 63–70.

[17] M. McCann, B. Coyle, S. McKay, P. McCormack, K. Kavanagh, M. Devereux, V. McKee, P. Kinsella, R. O'Connor, M. Clynes, Synthesis and X-ray crystal structure of $[Ag(phendio)_2]ClO_4$ (phendio = 1,10-phenanthroline-5,6-dione) and its effects on fungal and mammalian cells, Biometals 17 (2004) 635–645.

[18] A. Eshwika, B. Coyle, M. Devereux, M. McCann, K. Kavanagh, Metal complexes of 1,10-phenanthroline-5,6-dione alter the susceptibility of the yeast *Candida albicans* to amphotericin B and miconazole, Biometals 17 (2004) 415–422.

[19] C. Deegan, B. Coyle, M. McCann, M. Devereux, D.A. Egan, In vitro anti-tumour effect of 1,10-phenanthroline-5,6-dione (phendione), $[Cu(phendione)_3](ClO_4)_2 \cdot 4H_2O$ and $[Ag(phendione)_2]ClO_4$ using human epithelial cell lines, Chem. Biol. Interact. 164 (2006) 115–125.

[20] R. Rowan, T. Tallon, A.M. Sheahan, R. Curran, M. McCann, K. Kavanagh, M. Devereux, V. McKee, Silver bullets in antimicrobial chemotherapy: synthesis, characterisation and biological screening of some new Ag(I)-containing imidazole complexes, Polyhedron 25 (2006) 1771–1778.

[21] B. Thati, A. Noble, R. Rowan, B.S. Creaven, M. Walsh, M. McCann, D. Egan, K. Kavanagh, Mechanism of action of coumarin and silver(I)–coumarin complexes against the pathogenic yeast *Candida albicans*, Toxicol. Vitro 21 (2007) 801–808.

[22] S. Aslam, A.A. Isab, M.A. Alotaibi, M. Saleem, M. Monim-ul-Mehboob, S. Ahmad, I. Georgieva, N. Trendafilova, Synthesis, spectroscopic characterization, DFT calculations and antimicrobial properties of silver(I) complexes of 2,2'-bipyridine and 1,10-phenanthroline, Polyhedron 115 (2016) 212–218.

[23] M. McCann, A. Kellett, K. Kavanagh, M. Devereux, A.L.S. Santos, Deciphering the antimicrobial activity of phenanthroline chelators, Curr. Med. Chem. 19 (2012) 2703–2714.

[24] T. Kromp, W.S. Sheldrick, C. Näther, Network motifs and thermal properties of copper(I) halide and pseudohalide coordination polymers with 1,7- and 4,7-phenanthroline, Z. Anorg. Allg. Chem. 629 (2003) 45–54.

[25] A. Pavic, B.Đ. Glišić, S. Vojnovic, B. Warżajtis, N.D. Savić, M. Antić, S. Radenković, G.V. Janjić, J. Nikodinovic-Runic, U. Rychlewska, M.I. Djuran, Mononuclear gold(III) complexes with phenanthroline ligands as efficient inhibitors of angiogenesis: a comparative study with auranofin and sunitinib, J. Inorg. Biochem. 174 (2017) 156–168.

[26] N.D. Savić, B.Đ. Glišić, H. Wadepohl, A. Pavic, L. Senerovic, J. Nikodinovic-Runić, M.I. Djuran, Silver(I) complexes with quinazoline and phthalazine: synthesis, structural characterization and evaluation of biological activities, MedChemComm 7 (2016) 282–291.

[27] B.Đ. Glišić, L. Senerovic, P. Comba, H. Wadepohl, A. Veselinovic, D.R. Milivojevic, M.I. Djuran, J. Nikodinovic-Runic, Silver(I) complexes with phthalazine and quinazoline as effective agents against pathogenic *Pseudomonas aeruginosa* strains, J. Inorg. Biochem. 155 (2016) 115–128.

[28] N.D. Savić, D.R. Milivojevic, B.Đ. Glišić, T. Ilic-Tomic, J. Veselinovic, A. Pavic, B. Vasiljevic, J. Nikodinovic-Runic, M.I. Djuran, A comparative antimicrobial and toxicological study of gold(III) and silver(I) complexes with aromatic nitrogen-containing heterocycles: synergistic activity and improved selectivity index of Au(III)/Ag(I) complexes mixture, RSC Adv. 6 (2016) 13193–13206.

[29] U. Kalinowska-Lis, A. Felczak, L. Chęcińska, K. Zawadzka, E. Patyna, K. Lisowska, J. Ochocki, Synthesis, characterization and antimicrobial activity of water-soluble silver(I) complexes of metronidazole drug and selected counter-ions, Dalton Trans. 44 (2015) 8178–8189.

[30] C. Seward, J. Chan, D. Song, S. Wang, Anion dependent structures of luminescent silver(I) complexes, Inorg. Chem. 42 (2003) 1112–1120.

[31] K.N. Lazarou, I. Chadjistamatis, A. Terzis, S.P. Perlepes, C.P. Raptopoulou, Complexes derived from the copper(II)/succinamic acid/*N*,*N*′,*N*″-chelate tertiary reaction systems: synthesis, structural and spectroscopic studies, Polyhedron 29 (2010) 1870–1879.

[32] K.N. Lazarou, C.P. Raptopoulou, S.P. Perlepes, V. Psycharis, Complexes derived from the general copper(II)/maleamic acid/*N*,*N*′,*N*″-chelate reaction systems: synthetic, reactivity, structural and spectroscopic studies, Polyhedron 28 (2009) 3185–3192.

[33] D. Johnston, D.F. Shriver, Vibrational study of the trifluoromethanesulfonate anion: unambiguous assignment of the asymmetric stretching modes, Inorg. Chem. 32 (1993) 1045–1047.

[34] G.A. van Albada, W.J.J. Smeets, A.L. Spek, J. Reedijk, Synthesis, spectroscopic properties and X-ray crystal structures of two dinuclear alkoxo-bridged copper(II) compounds with the ligand bis(1-methyl-2-benzimidazolyl) propane. A unique alkoxo-bridged Cu(II) dinuclear compound with an additional bidentate bridging triflate anion, Inorg. Chim. Acta. 260 (1997) 151–161.

[35] A.M. Petrosyan, Vibrational spectra of L-histidine perchlorate and L-histidine tetrafluoroborate, Vib. Spectrosc. 43 (2007) 284–289.

[36] Q.-L. Ren, S.-S. Zhao, L.-X. Song, S.-S. Qian, J. Qin, Synthesis, characterization, and biological evaluation of silver(I) complexes of *N*′-(1-(pyrazin-2-yl)ethylidene)picolinohydrazide, J. Coord. Chem. 69 (2016) 227–237.

[37] A.S. Potapov, E.A. Nudnova, A.I. Khlebnikov, V.D. Ogorodnikov, T.V. Petrenko, Synthesis, crystal structure and electrocatalytic activity of discrete and polymeric copper(II) complexes with bitopic bis(pyrazol-1-yl)methane ligands, Inorg. Chem. Commun. 53 (2015) 72–75.

[38] A.B.P. Lever, E. Mantovani, B.S. Ramaswamy, Infrared combination frequencies in coordination complexes containing nitrate groups in various coordination environments. A probe for the metal-nitrate interaction, Can. J. Chem. 49 (1971) 1957–1964.

[39] U. Kalinowska-Lis, A. Felczak, L. Chęcińska, K. Lisowska, J. Ochocki, Synthesis, characterization and antimicrobial activity of silver(I) complexes of hydroxymethyl derivatives of pyridine and benzimidazole, J. Organomet. Chem. 749 (2014) 394–399.

[40] L. Yang, D.R. Powell, R.P. Houser, Structural variation in copper(I) complexes with pyridylmethylamide ligands: structural analysis with a new four-coordinate geometry index, τ_4, Dalton Trans. (2007) 955–964.

[41] D.L. Reger, E.A. Foley, M.D. Smith, Structural impact of multitopic third generation bis(1-pyrazolyl)methane ligands: double, mononuclear metallacyclic silver(I) complexes, Inorg. Chem. 49 (2010) 234–242.

[42] D.L. Reger, R.P. Watson, J.R. Gardinier, M.D. Smith, Impact of variations in design of flexible bitopic bis(pyrazolyl)methane ligands and counterions on the structures of silver(I) complexes: dominance of cyclic dimeric architecture, Inorg. Chem. 43 (2004) 6609–6619.

[43] C. Pettinari, F. Marchetti, G. Lupidi, L. Quassinti, M. Bramucci, D. Petrelli, L.A. Vitali, M.F.C.G. da Silva, L.M.D.R.S. Martins, P. Smoleński, A.J. Pombeiro, Synthesis, antimicrobial and antiproliferative activity of novel silver(I) tris(-pyrazolyl)methanesulfonate and 1,3,5-triaza-7-phosphadamantane complexes, Inorg. Chem. 50 (2011) 11173–11183.

[44] A. Heyneman, H. Hoeksema, D. Vandekerckhove, A. Pirayesh, S. Monstrey, The Role of Silver Sulphadiazine in the Conservative Treatment of Partial Thickness Burn Wounds: a Systematic Review, Burns, 42, 2016, pp. 1377–1386.

[45] M.N. Storm-Versloot, C.G. Vos, D.T. Ubbink, H. Vermeulen, Topical silver for preventing wound infection, Database Syst. Rev. 3 (2010). CD006478.

[46] B. Wächtler, F. Citiulo, N. Jablonowski, S. Förster, F. Dalle, M. Schaller, D. Wilson, B. Hube, *Candida albicans*-epithelial interactions: dissecting the roles of active penetration, induced endocytosis and host factors on the infection process, PLoS One 7 (2012) e36952.

[47] D.L. Moyes, D. Wilson, J.P. Richardson, S. Mogavero, S.X. Tang, J. Wernecke, S. Höfs, R.L. Gratacap, J. Robbins, M. Runglall, C. Murciano, M. Blagojevic, S. Thavaraj, T.M. Förster, B. Hebecker, L. Kasper, G. Vizcay, S.I. Iancu, N. Kichik, A. Häder, O. Kurzai, T. Luo, T. Krüger, O. Kniemeyer, E. Cota, O. Bader, R.T. Wheeler, T. Gutsmann, B. Hube, J.R. Naglik, Candidalysin is a fungal peptide toxin critical for mucosal infection, Nature 532 (2016) 64–68.

[48] R.K. Koiri, S.K. Trigun, S.K. Dubey, S. Singh, L. Mishra, Metal Cu(II) and Zn(II) bipyridyls as inhibitors of lactate dehydrogenase, Biometals 21 (2008) 117–126.

[49] A.J. Phillips, I. Sudbery, M. Ramsdale, Apoptosis induced by environmental stresses and amphotericin B in *Candida albicans*, Proc. Natl. Acad. Sci. U.S.A. 100 (2003) 14327–14332.

[50] https://www.drugs.com/monograph/silver-sulfadiazine.html.

[51] O. Gordon, T.V. Slenters, P.S. Brunetto, A.E. Villaruz, D.E. Sturdevant, M. Otto, R. Landmann, K.M. Fromm, Silver coordination polymers for prevention of implant infection: thiol interaction, impact on respiratory chain enzymes, and hydroxyl radical induction, Antimicrob. Agents Chemother. 54 (2010) 4208–4218.

[52] X. Han, X. Gao, Sequence specific recognition of ligand–DNA complexes studied by NMR, Curr. Med. Chem. 8 (2001) 551–581.

[53] S. Neidle, C.M. Nunn, Crystal structures of nucleic acids and their drug complexes, Nat. Prod. Rep. 15 (1998) 1–5.

[54] G. Bischoff, S. Hoffmann, DNA-binding of drugs used in medicinal therapies, Curr. Med. Chem. 9 (2002) 312–348.

[55] J.N. Lisgarten, M. Coll, J. Portugal, C.W. Wright, J. Aymami, The antimalarial and cytotoxic drug cryptolepine intercalates into DNA at cytosine–cytosine sites, Nat. Struct. Biol. 9 (2002) 57–60.

[56] S. Neidle, DNA minor-groove recognition by small molecules, Nature Prod. For. Rep. 18 (2001) 291–309.

[57] J. Ren, J.B. Chaires, Sequence and structural selectivity of nucleic acid binding ligands, Biochemistry 38 (1999) 16067–16075.

[58] R.M. Knegtel, J. Antoon, C. Rullmann, R. Boelens, R. Kaptein, MONTY: a Monte Carlo approach to protein–DNA recognition, J. Mol. Biol. 235 (1994) 318–324.

[59] K. Bastard, A. Thureau, R. Lavery, C. Prevost, Docking macromolecules with flexible segments, J. Comput. Chem. 24 (2003) 1910–1920.

[60] A.A. Adesokan, V.A. Roberts, V.K.W. Lee, R.D. Lins, J.M. Briggs, Prediction of HIV-1 integrase/viral DNA interactions in the catalytic domain by fast molecular docking, J. Med. Chem. 47 (2004) 821–828.

[61] V.A. Roberts, D.A. Case, V. Tsui, Predicting interactions of winged-helix transcription factors with DNA, Proteins 57 (2004) 172–187.

[62] R. Rohs, I. Bloch, H. Sklenar, Z. Shakked, Molecular flexibility in *ab initio* drug docking to DNA: binding-site and binding-mode transitions in all-atom Monte Carlo simulations, Nucleic Acids Res. 33 (2005) 7048–7057.

[63] B. Nordén, F. Tjerneld, Structure of methylene blue-DNA complexes studied by linear and circular dichroism spectroscopy, Biopolymers 21 (1982) 1713–1734.

[64] V.I. Ivanov, L.E. Minchenkova, A.K. Schyolkina, A.I. Poletayer, Different conformations of double-stranded nucleic acid in solution as revealed by circular dichroism, Biopolymers 12 (1973) 89–110.

[65] N. Shahabadi, S. Kashanian, Z. Ahmadipour, DNA binding and gel

electrophoresis studies of a new silver(I) complex containing 2,9-dimethyl-1,10-phenanthroline ligands, DNA Cell Biol. 30 (2011) 187–194.
[66] N.A. Kasyanenko, Z. Qiushi, M.S. Varshavskii, V.M. Bakulev, V.N. Demidov, DNA metal complexes and metallization of a macromolecule in solution, J. Struct. Chem. 58 (2017) 406–412.
[67] C.A. MacRae, R.T. Peterson, Zebrafish as tools for drug discovery, Nat. Rev. Drug Discov. 14 (2015) 721–731.
[68] C. Bandeira, J.M. Filho, K. de Almeida Ramos, Reversible cardiomyopathy secondary to amphotericin-B, Med. Mycol. Case Rep 13 (2016) 19–21.
[69] C. Koch, M. Wolff, M. Henrich, M.A. Weigand, C. Lichtenstern, F. Uhle, Cardiac effects of echinocandins in endotoxemic rats, Antimicrob. Agents Chemother. 60 (2016) 301–306.
[70] R.L. Page, C.L. O'Bryant, D. Cheng, T.J. Dow, B. Ky, C.M. Stein, A.P. Spencer, R.J. Trupp, J. Lindenfeld, Drugs that may cause or exacerbate heart failure: a scientific statement from the American Heart Association, Circulation 134 (2016) e32–e69.
[71] J. Gola, A. Skubis, B. Sikora, C. Kruszniewska-Rajs, J. Adamska, U. Mazurek, B. Strzalka-Mrozik, G. Czernel, M. Gagos, Expression profiles of genes related to melatonin and oxidative stress in human renalproximal tubule cells treated with antibiotic amphotericin B and its modified forms, Turk. J. Biol. 39 (2015) 856–864.
[72] K. Klimek, J. Strubirinska, G. Czernel, G. Ginalska, M. Gagos, *In vitro* evaluation of antifungal and cytotoxic activities as also the therapeutic safety of the oxidized form of amphotericin B, Chem. Biol. Interact. 256 (2015) 47–54.
[73] B. Chudzik, G. Czernel, A. Miaskowski, M. Gagos, Amphotericin B-copper(II) complex shows improved therapeutic index *in vitro*, Eur. J. Pharmaceut. Sci. 97 (2017) 9–21.
[74] P.V. Asharani, G.L.K. Mun, M.P. Hande, S. Valiyaveettil, Cytotoxicity and genotoxicity of silver nanoparticles in human cells, ACS Nano 3 (2009) 279–290.
[75] A. Massarsky, L. Dupuis, J. Taylor, S. Eisa-Beygi, L. Strek, V.L. Trudeau, T.W. Moon, Assessment of nanosilver toxicity during zebrafish (*Danio rerio*) development, Chemosphere 92 (2013) 59–66.
[76] G.K. Patra, I. Goldberg, S. De, D. Datta, Effect of the size of discrete anions on the nuclearity of a complex cation, CrystEngComm 9 (2007) 828–832.
[77] O.V. Dolomanov, L.J. Bourhis, R.J. Gildea, J.A.K. Howard, H. Puschmann, OLEX2: a complete structure solution, refinement and analysis program, J. Appl. Crystallogr. 42 (2009) 339–341.
[78] G.M. Sheldrick, SHELXT – integrated space-group and crystal-structure determination, Acta Crystallogr. A 71 (2015) 3–8.
[79] G.M. Sheldrick, Crystal structure refinement with SHELXL, Acta Crystallogr. C 71 (2015) 3–8.
[80] I.J. Bruno, J.C. Cole, P.R. Edgington, M. Kessler, C.F. Macrae, P. McCabe, J. Pearson, R. Taylor, New software for searching the Cambridge Structural Database and visualizing crystal structures, Acta Crystallogr. Sect. B Struct. Sci. 58 (2002) 389–397.
[81] Á. Jakab, S. Mogavero, T.M. Förster, M. Pekmezovic, N. Jablonowski, V. Dombrádi, I. Pócsi, B. Hube, Effects of the glucocorticoid betamethasone on the interaction of *Candida albicans* with human epithelial cells, Microbiology 162 (2016) 2116–2125.
[82] B. Wächtler, D. Wilson, K. Haedicke, F. Dalle, B. Hube, From attachment to damage: defined genes of *Candida albicans* mediate adhesion, invasion and damage during interaction with oral epithelial cells, PLoS One 6 (2011) e17046.
[83] L. Sun, K. Liao, C. Hang, D. Wang, Honokiol induces reactive oxygen species-mediated apoptosis in *Candida albicans* through mitochondrial dysfunction, PLoS One 12 (2017) e0172228.
[84] M.B. Hansen, S.E. Nielsen, K. Berg, Re-examination and further development of a precise and rapid dye method for measuring cell growth/cell kill, J. Immunol. Meth. 119 (1989) 203–210.
[85] C.I. Bayly, P. Cieplak, W.D. Cornell, P.A. Kollman, A well-behaved electrostatic potential based method using charge restraints for deriving atomic charges: the RESP model, J. Phys. Chem. 97 (1993) 10269–10280.
[86] H.R. Drew, R.M. Wing, T. Takano, C. Broka, S. Tanaka, K. Itakura, R.E. Dickerson, Structure of a B-DNA dodecamer: conformation and dynamics, Proc. Natl. Acad. Sci. U.S.A. 78 (1981) 2179–2183.
[87] G.M. Morris, R. Huey, W. Lindstrom, M.F. Sanner, R.K. Belew, D.S. Goodsell, A.J. Olson, AutoDock4 and AutoDockTools4: automated docking with selective receptor flexibility, J. Comput. Chem. 30 (2009) 2785–2791.
[88] Dassault Systèmes BIOVIA, Discovery Studio Modeling Environment, Release 2017, 2016.
[89] J. Nikodinovic, K.D. Barrow, J.A. Chuck, High yield preparation of genomic DNA from *Streptomyces*, Biotechniques 35 (2003) 932–936.
[90] OECD, OECD Guidelines for the Testing of Chemicals, Test No. 236, 2013.